geosciences

MDPI

Article

Stealth Metasomatism in Granulites from Ivrea (NW Italy): Hydration of the (Variscan) Lower Crust by Melt Flow

Stylianos Karastergios [1,*], Simona Ferrando [2,*], Barbara E. Kunz [3] and Maria Luce Frezzotti [1]

[1] Department of Earth and Environmental Sciences, University of Milano-Bicocca, Piazza della Scienza 4, 20126 Milano, Italy; maria.frezzotti@unimib.it
[2] Department of Earth Sciences, University of Turin, Via Valperga Caluso 35, 10125 Turin, Italy
[3] School of Environment, Earth and Ecosystems, Faculty of Science, Technology, Engineering and Mathematics, The Open University, Walton Hall, Milton Keynes MK6 6AA, UK; barbara.kunz@open.ac.uk
* Correspondence: s.karastergios@campus.unimib.it (S.K.); simona.ferrando@unito.it (S.F.)

Abstract: Granulites and associated dykes from the less well-studied southern Ivrea–Verbano Zone (around Ivrea town) are characterized by combining field, macro, micro and chemical (major and trace-element mineral composition) data to identify chemical and rheological variations in the lower crust that could be relevant for geodynamic implications. The Ivrea granulites are similar to those in the Lower Mafic Complex of the central Ivrea–Verbano Zone. The mafic lithologies experienced stealth metasomatism (pargasitic amphibole and An-rich plagioclase) that occurred, at suprasolidus conditions, by a pervasive reactive porous flow of mantle-derived orogenic (hydrous) basaltic melts infiltrated along, relatively few, deformation-assisted channels. The chemical composition of the metasomatic melts is similar to that of melts infiltrating the central and northern Ivrea–Verbano Zone. This widespread metasomatism, inducing a massive regional hydration of the lowermost Southalpine mafic crust, promoted a plastic behavior in the lowermost part of the crust during the Early Mesozoic and, ultimately, the Triassic extension of the Variscan crust and the beginning of the Alpine cycle.

Keywords: Ivrea–Verbano Zone; lower crust; stealth metasomatism; melt infiltration; porous flow; channelized flow; hornblendites; hydrous basaltic melt

Citation: Karastergios, S.; Ferrando, S.; Kunz, B.E.; Frezzotti, M.L. Stealth Metasomatism in Granulites from Ivrea (NW Italy): Hydration of the (Variscan) Lower Crust by Melt Flow. *Geosciences* **2024**, *14*, 218. https://doi.org/10.3390/geosciences14080218

Academic Editor: Salvatore Critelli

Received: 7 July 2024
Revised: 10 August 2024
Accepted: 14 August 2024
Published: 16 August 2024

1. Introduction

The role of the lower continental crust in the processes that govern the transition from the late orogenic stages, such as the extensional regime linked to the orogenic collapse, to a new Wilson cycle (e.g., continental drifting) still needs to be better investigated. In this geodynamic context, the underplating of large volumes of mafic magma induces associated chemical and rheological variations in the lower crust and the overlying middle crust, with consequences for the distribution of stress fields, and the genesis of some ore deposits. Nevertheless, evidence for melt–rock interactions and the characterization of the involved processes (porous flow vs. channeled flow) have not received a lot of attention until recently (e.g., [1–4]). Moreover, the interaction between melts and deep mafic plutons straddles the boundary between igneous and high-temperature metamorphic processes, making its study a frontier topic.

Well-preserved lower crust sections rarely outcrop (e.g., [5–10] and references therein). The Ivrea–Verbano Zone IVZ in northern Italy is a promising site to study the melt–rock interaction in the lower crust and its potential geodynamic consequences. It is one of the best-preserved middle- to lower-continental crustal sections in the world, in which distinct mafic magmatic pulses infiltrated a Variscan lower crust during the Permian orogenic collapse (e.g., [11–13]), and in which different geological evidence of the Mesozoic Alpine rifting are preserved [e.g., [14–17], and references therein]. The IVZ is subdivided into the northern (Finero Complex), central (Strona, Sesia and Sessera valleys), and southern (Ivrea and Baldissero) IVZ. Previous studies concentrated on the northern (e.g., [18–27])

and central IVZ [28–43], and references therein]. To our knowledge, the only recent paper on the southern IVZ is by Mazzucchelli et al. [44] on the Baldissero peridotites, whereas the mafic rocks outcropping in and around the Ivrea town have never been studied in detail.

In the present paper, we studied the granulite rocks of the southern IVZ. We report field, macro, micro, and chemical (major and trace-element mineral composition) evidence of "stealth" metasomatic hydration of a former dry mafic lower crust induced by a combination of channelized flux and porous flow of orogenic hydrous basalts, and discuss geodynamic implications.

2. Geological Setting

The Ivrea–Verbano Zone (IVZ), located in NW Italy, is a 130 km long and 10–50 km wide strip that extends from Ivrea up to Locarno (Figure 1). The IVZ belongs to the Southalpine domain of the Alps, i.e., the domain consisting of Variscan continental crust and constituting the Adria plate during the Triassic–Jurassic extensional tectonics responsible for the opening of the Tethys Ocean [15,45,46]. This domain, also known as the Southern Alps, was only marginally involved in the compressional tectonics responsible for the Tethys closure and continental collision generating the Alpine chain, and, so, it records a low-grade Alpine metamorphism that is traced only along tectonic structures [14], and references therein]. To the SE, the IVZ is separated from the Serie dei Laghi sequence (Southalpine Variscan mid-to-upper crust section) by the Permian transpressional shear zone of Cossato-Mergozzo-Brissago and by the subsequent Pogallo and Cremosina Lines. To the NW, a thick (1 km wide) mylonite zone called the Insubric Line (e.g., [47–49]) separates the IVZ from the Sesia Zone (i.e., a Variscan continental crust strongly involved in the Alpine tectonics). To the SW, near Ivrea town, a ductile deep fault named the Internal Canavese Line (e.g., [50]) separates the IVZ from the Canavese Zone, a Variscan continental crust recording a very low-grade Alpine metamorphism. The IVZ is subdivided into three units: (a) the Kinzigite Formation, (b) the Mafic Complex, and (c) the Ultramafic Massifs (Figure 1).

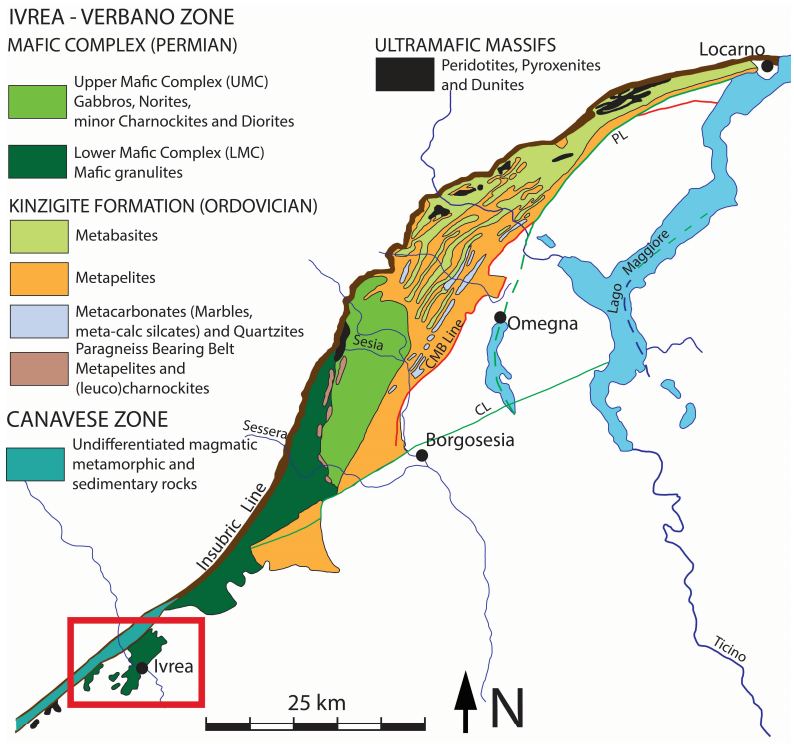

Figure 1. Simplified tectonic map of the western Southern Alps, Ivrea–Verbano Zone (IVZ); modified after [51]. The red rectangle represents the investigated area. Abbreviations: CMB = Cossato-Mergozzo-Brissago; PL = Pogallo Line; CL = Cremosina Line.

2.1. Kinzigite Formation

The Kinzigite Formation, well-exposed and studied in the Strona Valley, is mainly composed of alternating metapelites, metabasites, marbles, calc-silicates, and quartzites. This rock sequence has been shown to record the Variscan metamorphic evolution of the IVZ, where the metamorphic gradient increases perpendicular to the strike of the IVZ from SE to NW from amphibolite-to-granulite-facies metamorphism, respectively (e.g., [52–57]). The terms 'kinzigites' and 'stronalites' that will be used here were introduced by Schnetger [58] to describe amphibolite- and granulite-facies metapelites within the Kinzigite formation, respectively. The protolith composition is considered similar for both the granulite-facies and the amphibolite-facies metapelites in Strona Valley [59]. In the 1990s, the metabasic rocks within the Kinzigite formation were presumed to be part of the Mafic Complex (see below Section 2.2; e.g., [30,38,41,60]) on the basis of field and petrographic features. More recently, Kunz et al. [33] demonstrated that these rocks are, actually, pre-Variscan metabasalts [56,61] that experienced the same HT metamorphism and partial melting event as the associated metapelites.

The Variscan (316 ± 3 Ma; [36,62]) thermal peak in both metapelites [53] and metabasites [52] has been estimated at around 650–730 °C and ~3.5–6.5 kbar, for the amphibole-facies metamorphism, and up to 900–950 °C and ~10–12 kbar, for the granulite-facies metamorphism. Initially, the emplacement of the Mafic Complex was considered to be responsible for the granulitization of the overlying Kinzigite Formation (e.g., [32,55,63,64]). More recent geochronological and petrological data indicate an early Permian emplacement of the Mafic Complex (ca. 285 Ma, [65] more details below), i.e., a magmatism not synchronous with the Variscan thermal peak. To confirm this, a 2 km wide contact mineral assemblage has been observed to have overprinted the Variscan high-grade assemblages in the metapelites during the Permian (ca. 275 Ma; e.g., [37,53,63,66]).

2.2. Mafic Complex

The Mafic Complex is a large igneous body that intruded, at approximately 25 km depth, the Kinzigite Formation, in a post-Variscan transtensional tectonic setting (e.g., [11,60,63,67,68]). The Mafic Complex (MC) is a rather inhomogeneous intrusion interpreted to have been formed by separate magmatic pulses of mantle magma progressively contaminated by hosting Variscan restitic metapelites (stronalites) and by the anatectic melt generated in the more fertile host rocks due to crustal heating (e.g., [39] and references therein). The MC has been subdivided into two main units [41,42]: (a) the Lower Mafic Complex (LMC), mainly consisting of granoblastic, foliated amphibole gabbros, gabbronorites, and minor anhydrous charnockites; (b) the Upper Mafic Complex (UMC), which contains gabbronorites, diorites, and hydrous charnockites (in higher proportions compared to the LMC) with well-preserved magmatic structures. The Paragneiss–Bearing Belt (PBB) is the natural border between these two complexes and represents an arcuate-shaped zone, 1–2 km wide, rich in charnockites, norites, and ultramafic rocks alternating with metasedimentary septa considered as relics of the Kinzigite Formation [38,42,43,69]. The P-T conditions of crystallization of the MC are estimated at 8–9 kbar and 1000–1200 °C, whereas the granulitic re-equilibration was estimated at 850–950 °C ([63] and references therein). Very recently, U-Pb zircon geochronological data place the timing of the mafic intrusion during the early Permian (286–282 Ma), i.e., approximately 30 My after the peak metamorphic event recorded in the Kinzigite Formation [36,70]. Moreover, SHRIMP U-Th-Pb isotopic data indicate that the intrusion of the LMC started in the early Permian, at ca. 295 Ma, and experienced thermal recrystallization at around 285 Ma. The crystallization of the UMC occurred later, between 292 and 286 Ma, like that of the charnockites, which occurred at 277 Ma [39,65].

2.3. Ultramafic Massifs

Large bodies and smaller lenses and veins of ultramafic composition occur throughout the IVZ. The predominant lithologies are dunites, harzburgites, lherzolites, and, locally,

websterites with minor pyroxenites [71–73]. Three large ultramafic massifs are distinguished from NE towards SW: (a) Finero, (b) Balmuccia, and (c) Baldisero Canavese (Figure 1). The incorporation of these ultramafic massifs in the MC is quite enigmatic and several opinions exist in the literature [48,49,73]. Detailed field evidence suggests that the mantle peridotites have an igneous contact with the rocks of the MC, suggesting that the mantle peridotites are older than the mafic intrusion ([74] and references therein).

3. Methods

Both Energy Dispersive Spectrometry (EDS) and Wavelength Dispersive Spectrometry (WDS) data have been acquired on the studied samples. Scanning Electron Microscopy with Energy Dispersive Spectrometry (SEM-EDS) data were acquired using an SEM-JEOL JSMIT300LV, combined with an EDS Energy 200 system and an SDD X-Act3 detector (Oxford Inca Energy, Abingdon, UK), installed at the Department of Earth Sciences (University of Torino, Italy). The system is equipped with the Microanalysis Suite Oxford AZtecMineral and with the following analytical set-up: an accelerating voltage of 15 kV, a counting time of 50 s, a processing time of 3 µs, a working distance of 10 mm, and natural mineral standards. WDS data were gathered with a JEOL JXA 8200 Superprobe, equipped with five wavelength dispersive spectrometers, energy dispersive X-ray spectroscopy, and cathodoluminescence detectors, at the University of Milan. The operating conditions consisted of an acceleration voltage of 15 kV, at a beam current of 5 nA at 30 s counting time, with a spot size of 1 µm. For the calibration and the accuracy of the mineral analysis with the WDS, natural and synthetic minerals were used as standards. The cation distribution in the main petrogenetic minerals and the structural formulae were determined using the NORMPLUS software (v.2) of Ulmer [75] upgraded by S. Poli. Representative analyses are reported in Table S1.

Trace element data on the petrogenetic minerals (amphibole, plagioclase, orthopyroxene, clinopyroxene) from polished thin sections were determined using a Laser Ablation Inductively Coupled Plasma Mass Spectrometry (LA-ICP-MS) at the Open University (OU), UK. The instrument at the OU is a Photon Machines Analyte G2 with a 193 nm excimer laser, equipped with a HelEx II 2-volume cell, coupled with an Agilent 8800 ICP-QQQ-MS. The laser repetition rate of the analyses was at 10 Hz, 3.63 J/cm^2 fluence, and a spot diameter of 50 µm, which was reduced to 40 µm only for analyzing certain sites with interstitial plagioclase films. Representative analyses for each mineral can be found in Table S2.

Each analysis included 30 s of background measurement before ablation, 30 s of sample ablation, and a 40 s washout after the ablation. Detailed instrument and analytical conditions can be found in Table S3. The calibration strategy included the Standard Reference Material of the National Institute of Standards and Technology (SRM-NIST) 612 as a primary standard and Columbia River Basalt Glass (BCR-2G) as a secondary standard, which were analyzed every ~20 analyses. Data reduction was performed with the Iolite software, v3.71 [76]. The data quality of the BCR-2G analyses is in good agreement with published values [77] and with relative standard deviations of 0.47–22.88% (Table S4). Furthermore, probe data for major element concentrations were compared with major elements measured by LA-ICP-MS to ensure consistency between different methods. Element concentrations not plotted in the Rare Earth Element (REE) and trace element diagrams have values below the detection limit. For a full list of detection limits for each element, see Table S5.

4. Results

4.1. Field Evidence

In the area near Ivrea town, the IVZ mainly consists of mafic granulites and minor enderbites, with very rare metapelitic granulites (stronalites; Figure 2). These rocks are ubiquitous in the study area from Pavone Canavese and Lessolo, up to the contact with the Insubric Line, approximately 5–7 km north of Ivrea town. These rocks cover the NE part of the studied area, as well as the area around the villages of Fiorano and Pavone. The enderbites largely outcrop in the southeastern part of the studied area. The size and shape of

the enderbites can vary from the large and irregular bodies that are several hundred meters long and wide, outcropping at Monte Marino and Bric Appareglio, up to the very thin (<10 m) dykes which can be traced for several hundred meters and sporadically outcrop in the area between Ivrea and Lago Sirio. Where visible, the contact between mafic granulites and enderbites is usually transitional intrusive (see below). The stronalites outcrop only in the area between Ivrea and Lago Sirio and constitute decametric-thick septa, apparently aligned in a SW–NE direction, within the mafic granulites. Moving towards the contact with the Insubric Line (i.e., the Internal Canavese Line), the lithologies are progressively fine-grained and mylonitized.

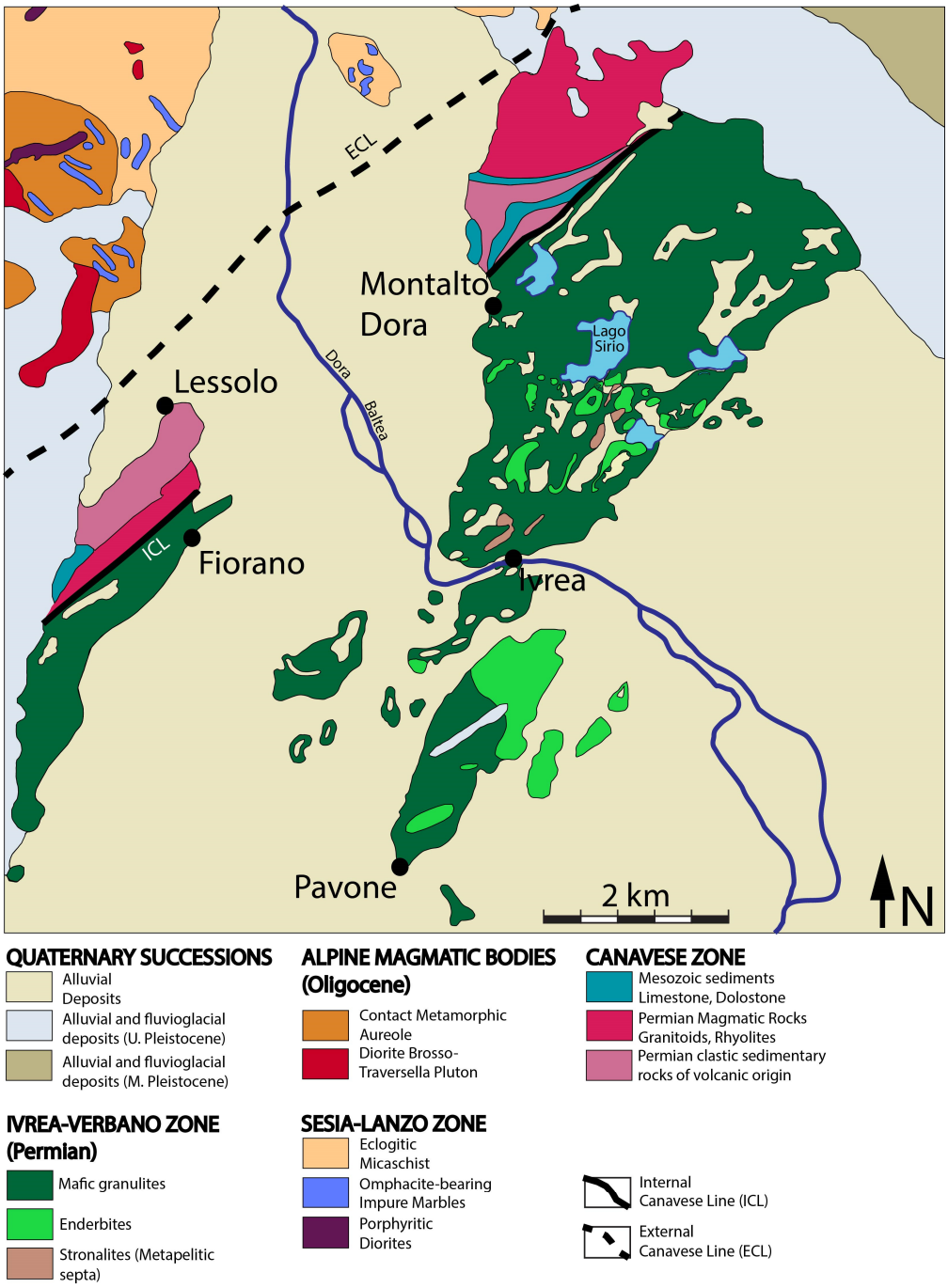

Figure 2. Simplified geological map of the studied area. ICL = Intenral Canavese Line; ECL = External Canavese Line.

Below, the field appearance and relationships among mafic granulites, enderbites, and stronalites are described in detail. More than 60 thin sections from collected samples and samples already present in the collection at the University of Turin have been characterized under an optical microscope. Five samples were selected for more detailed analyses (Table 1). The mineral abbreviations used in the text and the figures are from Whitney and Evans [78].

Table 1. Selection of representative samples from the SW Ivrea–Verbano zone. Underlined samples were selected for more detailed analysis.

Sample Name	Coordinates (N, E)	Specimen Description
IZ21-01	45°26′47″, 7°52′48″	Medium-grained enderbite
IZ21-02	45°26′47″, 7°52′47″	Coarse-grained enderbite
IZ21-03	45°26′47″, 7°52′46″	Coarse-grained enderbite in contact with fine-grained enderbitic dyke
IZ21-04	45°26′51″, 7°52′53″	Very coarse-grained enderbite
IZ21-06	45°28′29″, 7°52′49″	Fine-grained stronalite
IZ21-07	45°28′29″, 7°52′50″	Medium-grained stronalite
IZ21-13	45°28′37″, 7°52′55″	Medium-grained stronalite with cm-sized Grt porphyroblasts
IZ21-14	45°26′41″, 7°51′50″	Coarse-grained mafic granulite with pegmatoid coarse-grained lens
IZ21-15	45°26′41″, 7°51′50″	Cpx-rich band in contact with sample IZ21-14
IZ21-17	45°26′41″, 7°51′50″	Coarse-grained Amp-rich mafic granulite
IZ21-18	45°26′40″, 7°51′49″	Coarse-grained mafic granulite
IZ21-19	45°26′39″, 7°51′49″	Anhydrous coarse-grained mafic granulite
IZ21-20	45°26′39″, 7°51′48″	Foliated coarse-grained mafic granulite
IZ21-21	45°26′40″, 7°51′49″	Slightly foliated medium-grained mafic granulite with Cpx porphyroblasts
IZ21-22	45°26′37″, 7°51′56″	Medium- to coarse-grained mafic granulite, rich in opaques
IZ21-23	45°26′27″, 7°51′39″	Homogeneous medium- to coarse-grained mafic granulite
IZ23-02b	45°28′19″, 7°52′58″	Slightly foliated Amp–Cpx-poor mafic granulite with a pyroxenitic layer

4.1.1. Mafic Granulites

The mafic granulites macroscopically exhibit an apparent homogenous texture and composition ranging from gabbronorite to amphibole gabbronorite (Amp–gabbronorite). However, a detailed examination revealed local variations in grain size (from medium- to coarse-grained; Figure 3A,B), in texture (from granoblastic to faintly foliated; Figure 3A,B), and in modal composition (variation in Pl and Amp contents, Figure 3C). Locally, the mafic granulites exhibit 0.5–5 cm-wide pyroxene-rich layers showing infiltrating plagioclase (Pl) from the selvages, and fractures filled by infiltrated coarse-grained Pl + Amp (Figure 3C,D). The mafic granulites are crosscut by enderbites and Amp-rich dykes (see below).

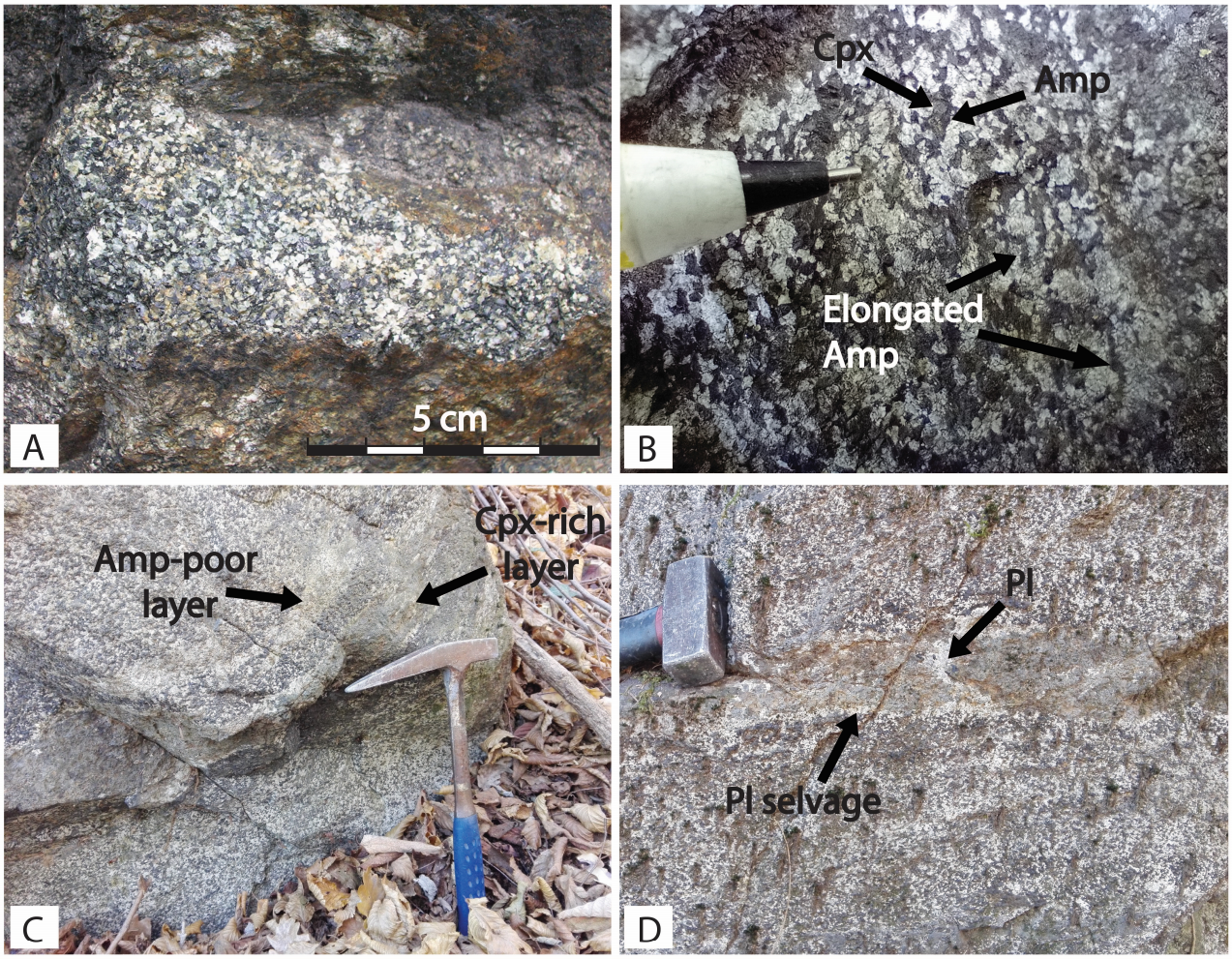

Figure 3. Mafic granulite field appearance. (**A**) Typical medium- to coarse-grained granoblastic mafic granulite mainly consisting of Pl and Amp in similar modal proportion. Locality: Ivrea market. (**B**) Coarse-grained faintly foliated mafic granulite in which a green, with a grayish hue, clinopyroxene (Cpx), is surrounded by black Amp. The foliation is locally marked by elongated Amp (black arrow). Locality: Ivrea, Beneficio di S. Lucia road. (**C**) Coarse-grained granoblastic mafic granulite showing dismembered Cpx-rich layers (arrows). The selvages blend gradually into the granulites or are marked by Pl. Locality: Ivrea, Bric Appareglio. (**D**) Detail of a Cpx-layer within medium-grained granoblastic mafic granulite. The layer is cut and infiltrated by coarse-grained Pl and minor Amp, and the selvages are marked by infiltrating Pl. Locality: Ivrea, Bric Appareglio. The mineral abbreviations are after [78].

4.1.2. Enderbites

The enderbites are predominantly medium- to coarse-grained and granoblastic (Figure 4A). A local faint foliation marked by orthopyroxene (Opx), up to ~0.5 mm long, is also common, regardless of the grain size of these rocks (Figure 4B). Fine-grained enderbites appear as sporadic dykes, less than 10 cm in width, that crosscut the coarser-grained enderbites (Figure 4C). The selvages are straight and do not show any chemical reaction with the host enderbite. Fine-grained enderbitic dykes are also found to crosscut the mafic granulites (Figure 4D). The observed selvages are usually overprinted by the Alpine orogeny, but they seem to lack evidence for reactions with the host mafic granulites.

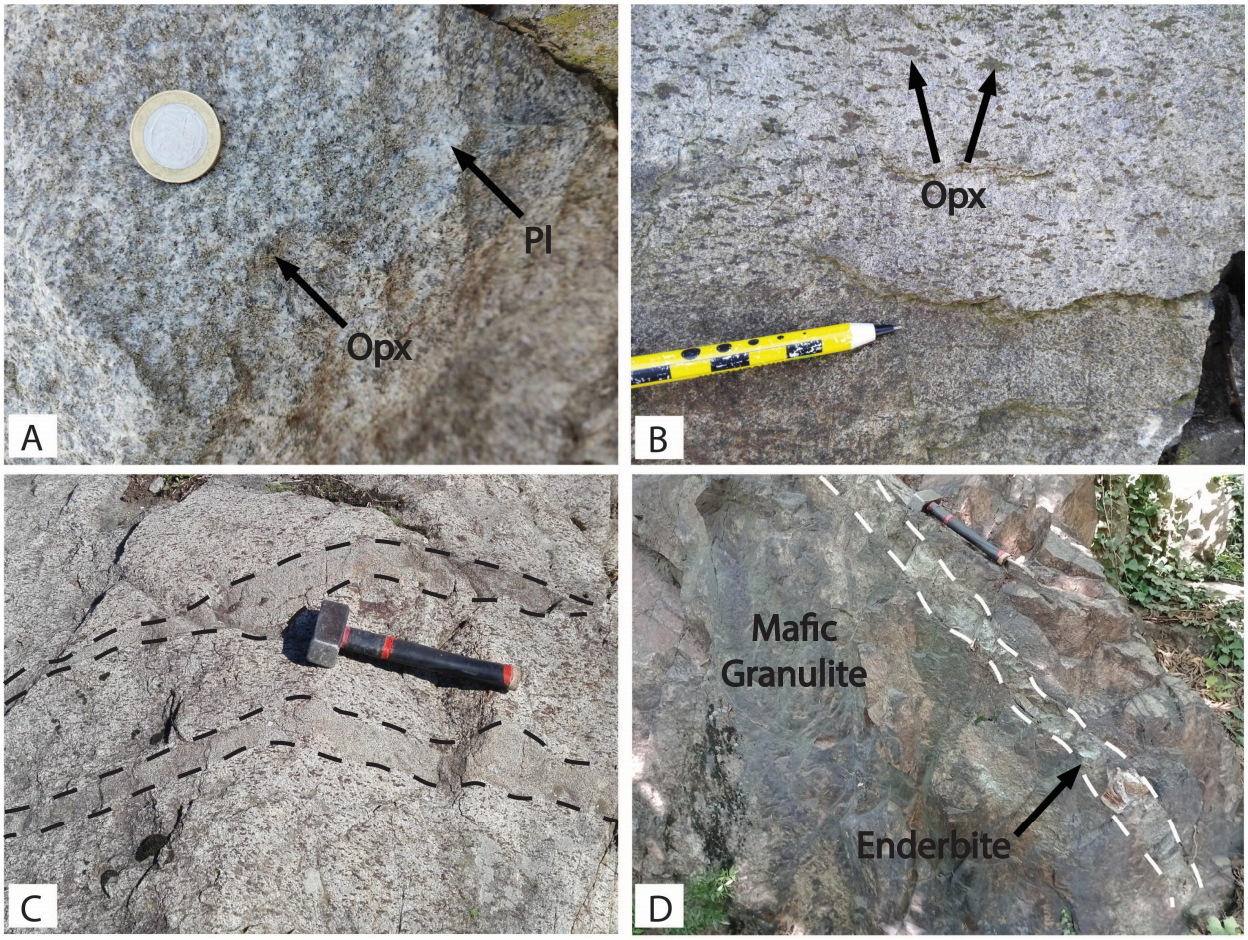

Figure 4. Enderbite field appearance. (**A**) Typical medium-grained granoblastic enderbite mainly consisting of Pl and orthopyroxene (Opx). Locality: Ivrea, Monte Marino Road. (**B**) Faintly foliated enderbite in which the foliation is marked by coarse-grained elongated Opx. Locality: Ivrea, Monte Marino Road. (**C**) Fine-grained enderbitic dykes within coarse-grained enderbite. Locality: Ivrea, Monte Marino Road. (**D**) Fine-grained enderbitic dyke within medium-grained mafic granulite. Locality: Ivrea, Monte Stella Road.

Enderbites outcropping in Ivrea town, particularly those located north of the river Dora Baltea, are fine-grained, richer in quartz (Qz) (>20 vol%), and poorer in Opx (<10%) compared to the enderbites outcropping in the southern part of the studied area. According to the QAP diagram for Opx-bearing granitic rocks [79], the threshold for quartz to classify a rock as a true enderbite is 20 vol%. The enderbites from the southern area do not contain as much quartz (~5–6 vol%) and, therefore, should be classified as "Opx-diorite or Opx-granitoid" [79]. However, because of similar field relationships, microstructures, and mineral assemblage, we consider these rocks as a more mafic variety of the Ivrea enderbites.

4.1.3. Amphibole-Rich Dykes, Pods, and Lenses

Both mafic granulites and enderbites are infiltrated by Amp-rich elongated dykes, pods, or lenses (Figure 5) that show irregular (Figure 5A,C) or gradual (Figure 5B,D) contacts. Usually, the Amp-rich dykes show a hypidiomorphic granular structure from coarse-grained (Figure 5C,D) to pegmatitic (Figure 5A,B). The Pl content is variable, but always significantly lower than in the mafic granulites (Figure 5C,D). The composition of the Amp-rich dykes ranges from Amp–gabbronorite to hornblendite.

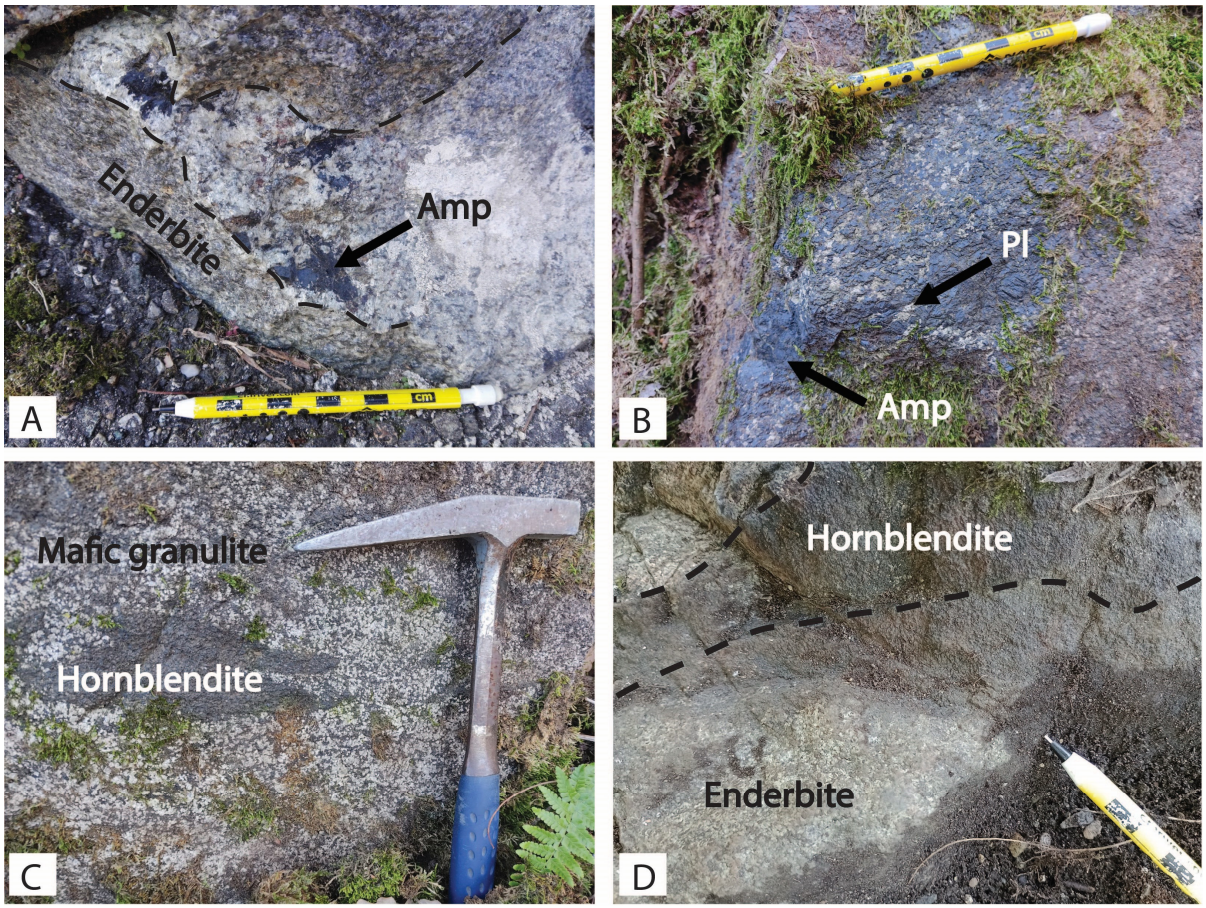

Figure 5. Amp-rich dykes and pods field appearance. (**A**) Pegmatoid Amp-rich dyke crosscutting enderbite with straight contact. Locality: Ivrea, Monte Marino Road. (**B**) Coarse-grained Amp-rich pod gradually fading into mafic granulite. Locality: Ivrea, Bric Appareglio. (**C**) Coarse-grained hornblenditic lens within mafic granulite. Locality: Ivrea, Bric Appareglio. (**D**) Medium-grained hornblenditic dyke crosscutting the enderbite with a straight contact. Locality: Ivrea, Monte Stella Road.

4.1.4. Quartz-Feldspathic Dykes

Locally, both mafic granulites and enderbites are crosscut by coarse-grained quartz-felspathic dykes that show straight contacts (Figure 6A). Crosscutting relationships with the Amp-rich dykes are not observed.

4.1.5. Stronalites

The stronalites are rare and outcrop in the central part of the studied area (Figure 2). They constitute a few 'septa' (i.e., thin, lensoidal bodies that can be traced for a rather long distance) up to 100 m long and 20–50 m wide. The septa appear oriented ca. NE–SW (Figure 2), i.e., parallel to the main strike observed in other localities of the IVZ (Figure 1). The stronalites are usually intercalated between enderbites and mafic granulites, however, their contact is not visible. The stronalites exhibit partial melting structures, such as leucosome formation, melt segregation, and the formation of coarse-grained quartz veins (Figure 6B). The quartz veins commonly have an amethyst-like color, due to numerous inclusions of rutile needles. The coarse-grained stronalites contain garnet porphyroblasts up to 1 cm in diameter (Figure 6B), while the fine-grained varieties contain plagioclase and garnet < 0.5 mm in diameter. Plagioclase and sillimanite, both fibrolitic and prismatic, are abundant, but very minor K-feldspar and biotite are also observed. The stronalites are usually not well preserved and show extended plagioclase alterations and retrograde

quartz + scapolite or quartz + (clino)zoisite veins. Further investigation of the stronalitic septa is beyond the scope of this work.

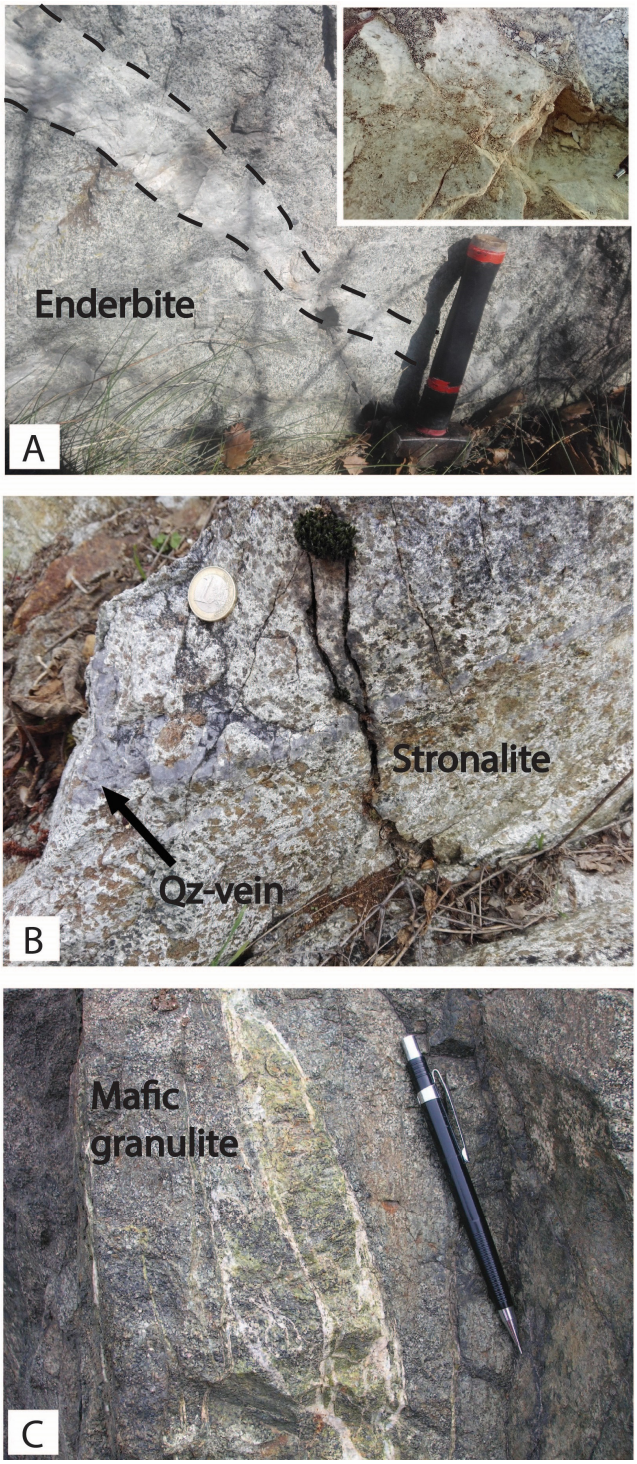

Figure 6. Field appearance of other, minor lithologies. (**A**) Coarse-grained quartz-felspathic dyke crosscutting enderbite with straight contact. Locality: Ivrea, Campagna Lake. The inset shows a close-up image of a quartz-feldspathic dyke crosscutting mafic granulites. Locality: Ivrea, Monte Stella Road. (**B**) Stronalite outcrop showing cm-wide porphyroblastic garnet and cm-thick quartz (Qz)-vein. The Qz grayish color is due to inclusions of rutile needles. Locality: Ivrea, Canton Gabriel Road. (**C**) Cm-thick Alpine vein consisting of green epidote + plagioclase + chlorite (Ep + Pl + Chl) within mafic granulite. Locality: Ivrea market.

4.1.6. Alpine Overprint

The field evidence of the Alpine overprint increases moving towards the contact with the Insubric Line, near Montalto Dora (Figure 2), and it is represented by ductile (mylonites) and fragile (cm-thick Chl-Pl-Ep veins) structures and by replacement of the mafic minerals by a very-low-grade mineral assemblage (Figure 6C).

4.2. Petrography, Mineral Chemistry, and Thermobarometry

4.2.1. Mafic Lithologies

The sampled mafic granulites display a medium- to coarse-grained (~1 mm in diameter) granoblastic texture that is locally polygonal, although faintly foliated samples are also present. Locally, relic magmatic structures are still well recognizable. These rocks consist of plagioclase, orthopyroxene, clinopyroxene, and variable modal amounts of amphibole. The accessory minerals include opaques (magnetite and ilmenite), spinel (hercynite, hereafter Hc), and apatite. Sample IZ23-02b has low Cpx content and the mineral composition is intermediate between the more mafic samples and the enderbitic ones (see below). Millimeter-to-centimeter thick pyroxene-layers parallel to the main foliation locally occur (Figure 7A).

Two generations of Pl and pyroxenes (Px) can be easily distinguished. The first one consists of coarse-grained (2–9 mm) porphyroclasts of Pl, Opx, and Cpx with lobate grain boundaries, while the second one consists of medium- to fine-grained neoblasts with a granoblastic polygonal structure (Figure 7B). The cores of porphyroclastic Pl include apatite (Ap) and Px and are the richest in Na (An = 0.59–0.65; Figure 8a), although the composition varies from one sample to another. The Pl neoblasts and the rims of the porphyroclasts are almost devoid of mineral inclusions, and their composition is always slightly higher in Ca with respect to the corresponding porphyroclastic cores (An = 0.64–0.67; Figure 8a). Another Pl generation constitutes μm-wide interstitial films between Cpx and Mag ± Hc (Figure 7C–E) and, very rarely, between Opx and Mag ± Hc, but not between Amp and Mag ± Hc (Figure 7E). The composition of this generation is the highest in Ca and shows a large An spread (An = 0.76–0.88; Figure 8a). In sample IZ21-20a (foliated mafic granulite), the Pl neoblasts show a chemical re-equilibration towards the more calcic compositions of the interstitial Pl (Figure 8a).

Both Opx generations are characterized by evident pleochroism from light green to light pink (Figure 7B). The Opx porphyroclasts show dark brown exsolution lamellae of a probable opaque phase (Figure 7F), whereas the neoblasts lack exsolutions (Figure 7B). The Opx porphyroclastic cores show higher Ca contents (>0.028 a.p.f.u.) than both the porphyroclastic rims and the neoblasts (<0.024 a.p.f.u.), whereas the Mg# is constant (0.69–0.70 in the porphyroclastic cores and 0.68–0.72 in the porphyroclastic rims and neoblasts; Figure 9a). The Al contents are more scattered, but usually higher in the porphyroclasts (>0.217 a.p.f.u) than in the neoblasts (Figure 9b). In the Amp–Cpx-poor sample (IZ23-02b), Opx has lower, but overlapping, Mg# values (from 0.59 to 0.61) in the porphyroclasts (cores and rims) and the neoblasts. The Ca contents are similar to the porphyroblastic rims and neoblasts from the other mafic granulites (<0.026 a.p.f.u.), while the Al contents are significantly lower compared to analyses from the other mafic granulites (<0.109 a.p.f.u.; Figure 9a,b).

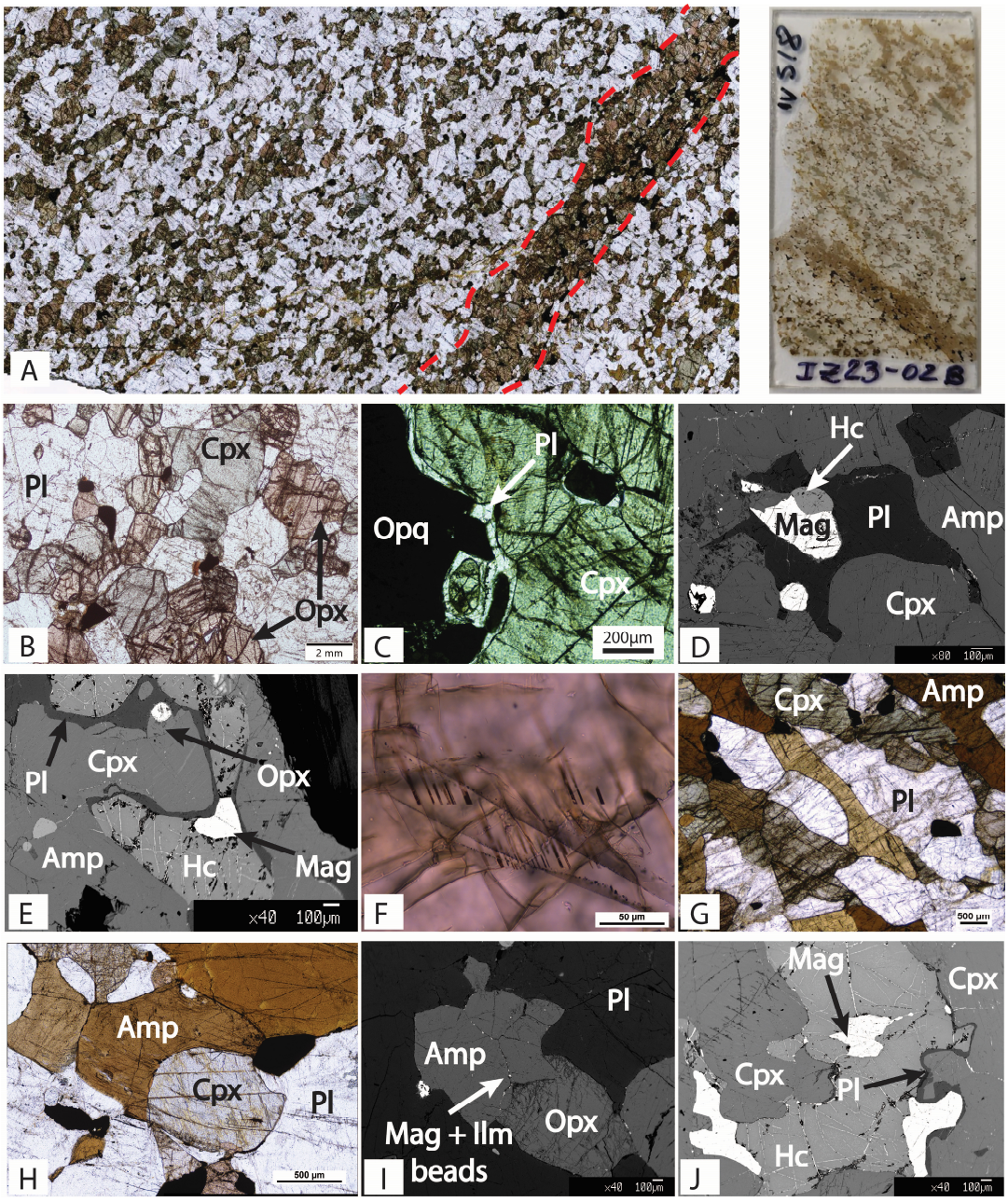

Figure 7. Mafic granulites under the microscope. (**A**) Scan (**right**) and panoramic photomicrograph (**left**) on plane-polarized light (PPL) of an Amp–Cpx-poor mafic granulite with a pyroxenitic band parallel to the rock foliation (sample IZ23-02b). Variations in grain size, in modal amounts of pyroxenes, and in amphibole are recognizable. (**B**) Photomicrograph showing porphyroclastic Pl and pyroxenes with lobate grain-boundaries in associations with smaller granoblastic neoblasts. Sample IZ23-02b, PPL. (**C**) Interstitial Pl (white arrow) filling the grain boundary between opaques (Opq) and Cpx. Sample IZ21-17, PPL. (**D**) Interstitial Pl on Mag and on rounded exsolution-rich Cpx. Sample IZ21-17, back-scattered electron image (BSE). (**E**) Interstitial Pl between pyroxenes and Hc or Mag, but not between Hc and Amp. Note the Opx exsolution lamellae within porphyroclastic Cpx. Sample IZ21-17, BSE. (**F**) Typical brown exsolutions within porphyroclastic Opx. Sample IZ21-20a, thick section, PPL. (**G**) Interstitial Amp between Pl-Pl and Opx-Cpx grain boundaries. Sample IZ21-20a, PPL (**H**) Rounded Cpx partly replaced by interstitial Amp. Sample IZ21-18a, PPL. (**I**) Granoblastic polygonal Amp with ilmenite ± magnetite (Ilm ± Mag) "beads" at the grain boundaries. Sample IZ21-18a, BSE. (**J**) Allotriomorphic Mag partly preserved from Hc substitution. Note the Pl continuous film at the contact between Cpx and Mag or Hc. Sample IZ21-17, BSE.

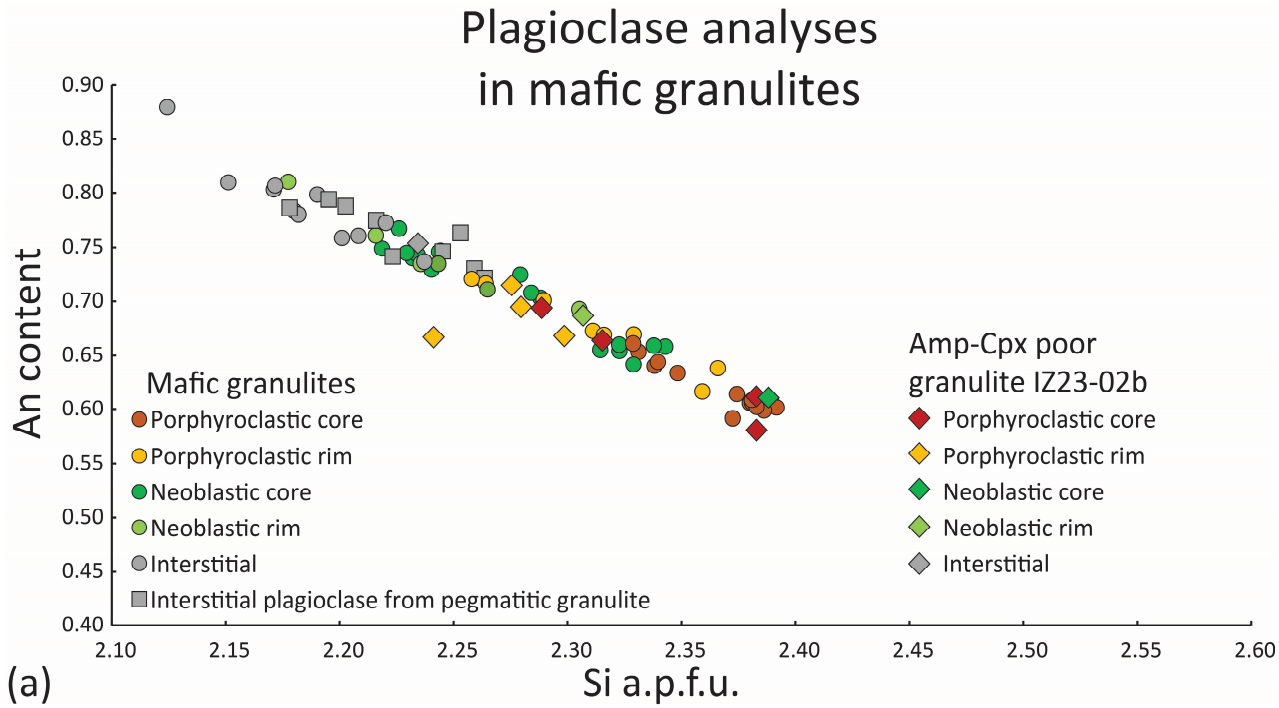

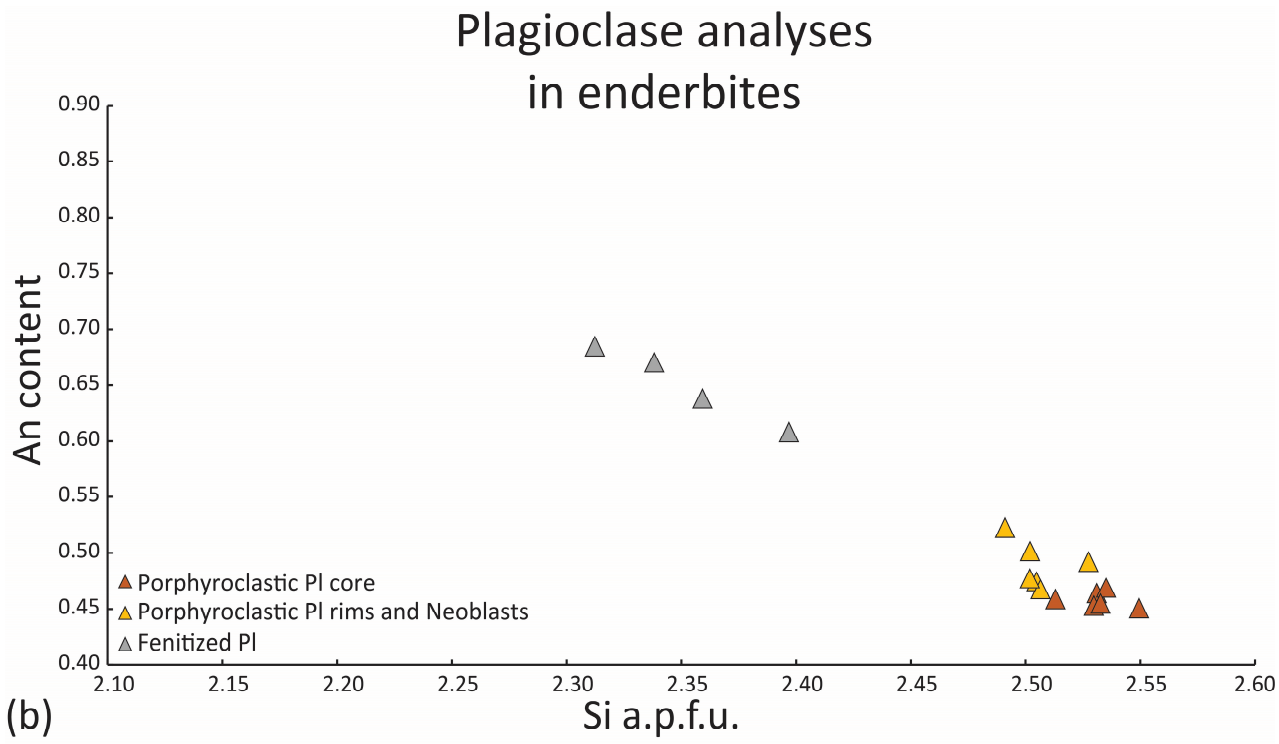

Figure 8. Plagioclase chemical composition in mafic granulite and Amp–Cpx-poor granulite (**a**) and in enderbite (**b**).

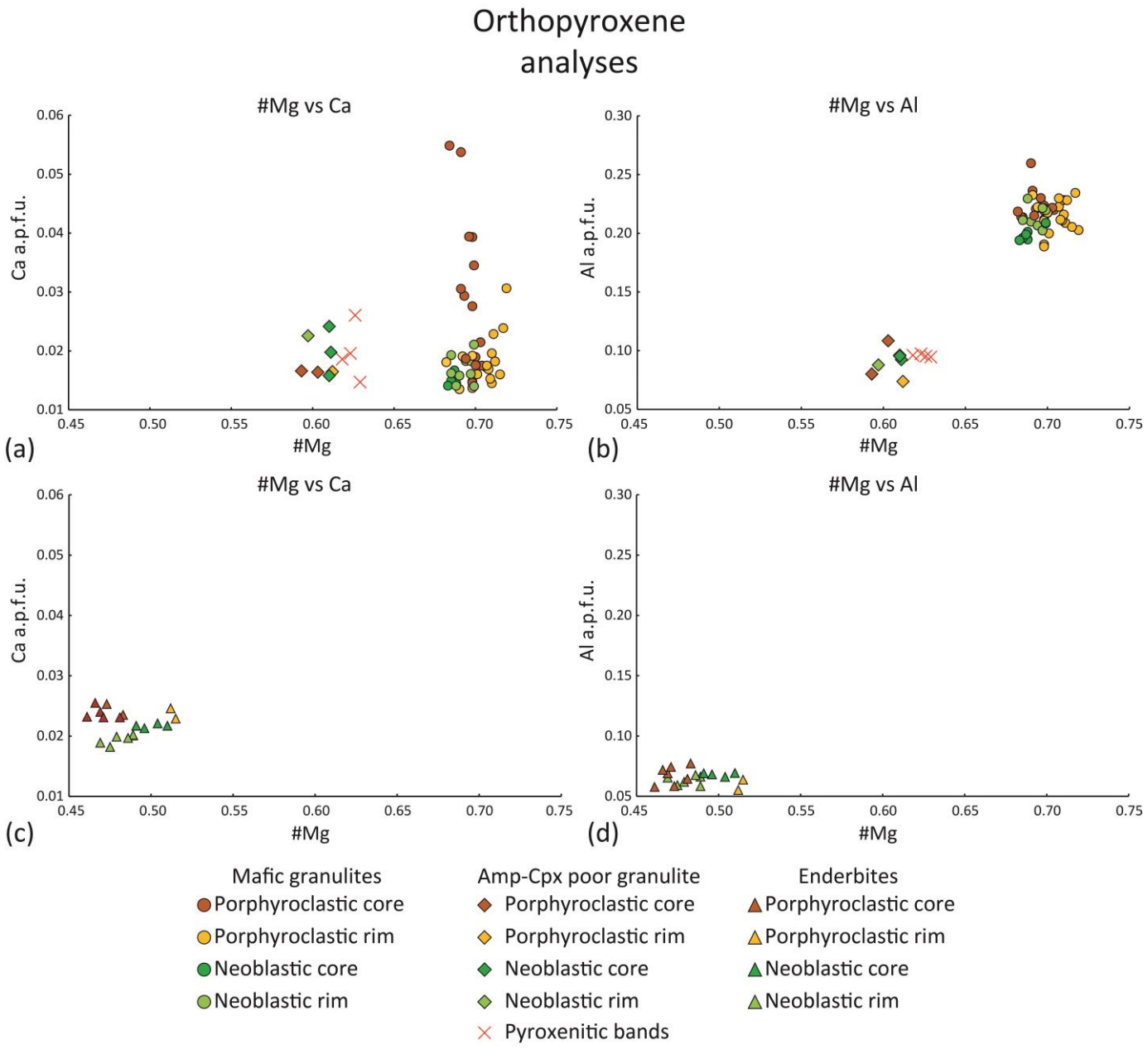

Figure 9. Orthopyroxene chemical composition in mafic granulite and Amp–Cpx-poor granulite (**a**,**b**) and in enderbite (**c**,**d**).

The Cpx is pale green and not pleochroic (Figure 7B). The Cpx porphyroclasts usually contain opaque minerals and show exsolution lamellae of Opx (Figure 7B,D,E), but the neoblasts lack exsolution lamellae (Figure 7B). The Cpx is diopside with variations in composition not related to the different generations. The Mg# values range from 0.75 to 0.81, the Ca contents from 0.83 to 0.87 a.p.f.u., the Al contents from 0.26 to 0.32 a.p.f.u., the Ti contents from 0.015 to 0.026 a.p.f.u., and the Na contents from 0.050 to 0.067 a.p.f.u. (Figure 10). In the Amp–Cpx-poor sample (IZ23-02b), clinopyroxene has lower Mg# (around 0.72), whereas the Ca contents range from 0.87 to 0.88 a.p.f.u., the Al contents are around 0.14 a.p.f.u., the Ti contents are 0.01 a.p.f.u., and the Na contents range from 0.03 to 0.04 a.p.f.u. (Figure 10).

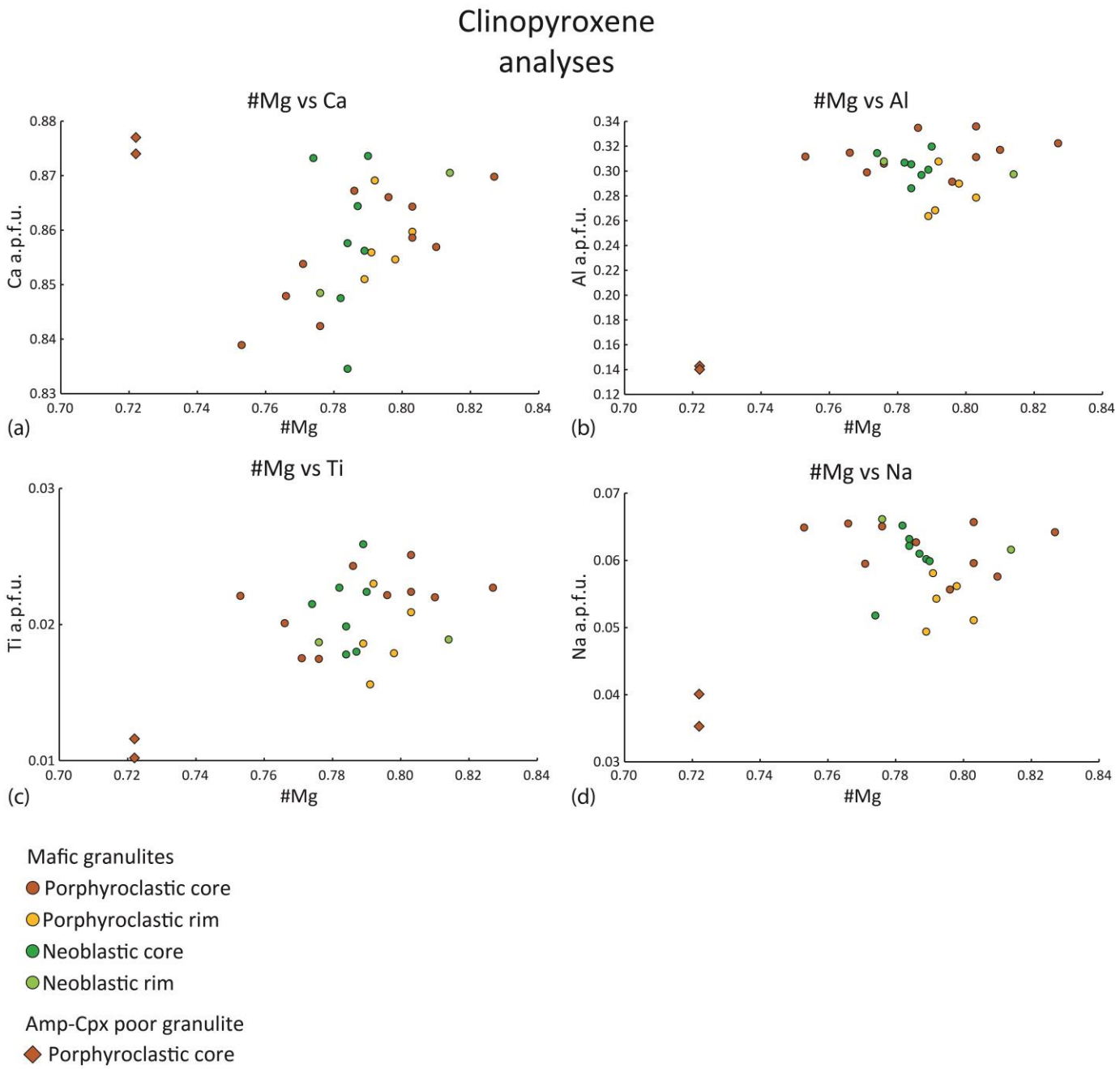

Figure 10. Clinopyroxene chemical composition in mafic granulite and Amp–Cpx-poor granulite. Correlation of the #Mg with (**a**) Ca a.p.f.u., (**b**) Al a.p.f.u., (**c**) Ti a.p.f.u., and (**d**) Na a.p.f.u.

Brown Amp is medium-to-coarse-grained and shows pleochroism from pale brown to dark brown. It constitutes (i) large interstitial crystals, usually with shape preferred orientation, between Pl–Pl or Px–Px grain boundaries (Figure 7G) and partly replaces rounded Cpx (Figure 7H); (ii) granoblasts with Ilm ± Mag "beads" at the Amp–Amp triple joints (Figure 7I). The chemical compositions overlap and correspond to a Ti-rich pargasite characterized by Mg# = 0.65–0.73, and (in a.p.f.u.) Ca = 1.70–1.84, Mn = 0.02–0.03, Al = 2.48–2.67, K = 0.12–0.24, Na = 0.74–0.90, Ti = 0.31–0.41, Cl $\leq$ 0.02, and F $\leq$ 0.12 (Figure 11). In the Amp–Cpx-poor sample (IZ23-02b), Amp has lower Mg# (0.60–0.67), and (in a.p.f.u.) Ca = 1.83–1.87, Mn = 0.003–0.017, Al = 2.25–2.34, K = 0.32–0.42, Na = 0.31–0.49, Ti = 0.19–0.28, Cl $\leq$ 0.07, and F = 0.19–0.31 (Figure 11). Nomenclature diagrams for plagioclase, pyroxenes, and amphibole can be found in the Supplementary Figure S1.

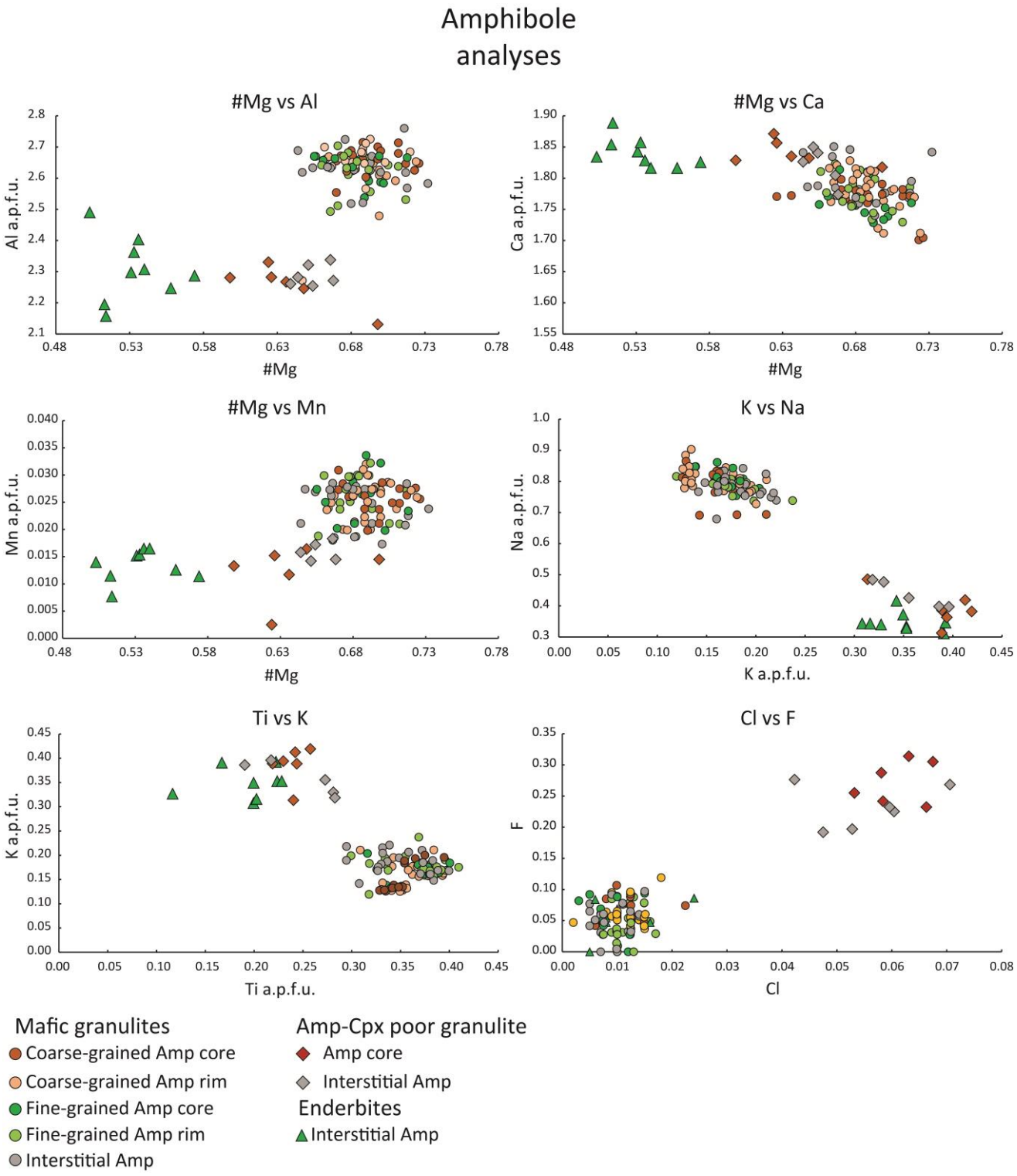

Figure 11. Amphibole chemical composition in mafic granulite, Amp–Cpx-poor granulite and enderbite.

The Mag is usually associated with pyroxenes and constitutes allotriomorphic or polygonal crystals (Figure 7J), depending on the rocks' structure. It appears as blebs inside composite crystals with deep green Hc, partially surrounded by interstitial Pl (Figure 7J).

The Px-rich layers are medium- to very coarse-grained and consist of Opx, Cpx, and variable amounts of Mag, Ilm, and Pl (Figure 12A). The layers exhibit a granoblastic

structure; however, the parent magmatic structure is still commonly preserved. Both Cpx and Opx show exsolution lamellae and opaque minerals show interstitial or polygonal habit. Opx from the pyroxenitic layer of sample IZ23-02b has a relatively homogeneous composition with Mg# = 0.62–0.63, Ca content ranging from 0.015 to 0.026 a.p.f.u., and Al content less than 0.1 a.p.f.u. (Figure 9a,b). The associated Pl in the pyroxenitic layers has an anorthite content ranging from 0.62 to 0.66, while interstitial Pl reaches An = 0.75. Locally, the layers are infiltrated by coarse-grained brown Amp + Pl (Figure 12B) that exhibit the interstitial structures already described for the mafic granulites (Figure 12C,D). These structures are well preserved in the samples that correspond to the coarse-grained Amp-rich elongated bodies, pods, or lenses, locally pegmatitic, that infiltrate both mafic granulites and Px-rich layers. These lithologies show increased proportions in brown Amp and/or Pl (Figure 12E) and usually exhibit interstitial or granoblastic structures. In particular, the Amp–Amp triple joints are marked by the Ilm ± Mag "beads" already described for the mafic granulites (Figure 12F). The interstitial Pl is Ca-rich (An = 0.72–0.79), like the interstitial Pl within the mafic granulites (Figure 8a). Interstitial Amp and neoblasts have overlapping compositions of a Ti-rich pargasite characterized by Mg# = 0.67–0.72, and (in a.p.f.u.) Ca = 1.73–1.82, Mn = 0.02–0.03, Al = 2.49–2.67, K = 0.17–0.22, Na = 0.74–0.84, Ti = 0.30–0.36, and Cl = 0.01–0.02; F $\leq$ 0.10 (Figure 11). These compositions are similar to those of the Amp from mafic granulites, but are characterized by slightly higher K and lower Ti contents (Figure 11).

4.2.2. Enderbites

The enderbites from Ivrea range from fine-grained (dykes) to very coarse-grained (~1 mm in size) with local faint foliation defined by Opx, either as elongated porphyroclasts (Figure 13A) or as neoblastic aggregates (Figure 13B). The mineral assemblage mainly consists of Pl, Opx, and Opq ± Qz ± Amp. Although relict porphyroclastic Pl and Opx exhibit lobate grain boundaries (Figure 13C), the more abundant neoblasts show granoblastic texture with triple joints (Figure 13D).

The composition of the cores of porphyroclastic Pl are the Na-richest (An = 0.45–0.47; Figure 8b), whereas the porphyroclastic rims and the neoblasts are slightly Ca-richer (An = 0.47–0.52; Figure 8b). Locally, the Pl contain, in their interior or at their grain boundaries, irregularly shaped Qz blebs that exhibit uniform extinction (Figure 13E) and are closely associated with replacement antiperthitic K-feldspar (Kfs; Figure 13F). The Pl composition around the blebs and replacement antiperthites are enriched in anorthitic components (An = 0.61–0.69; Figure 8B).

The Opx constitutes two generations: the porphyroclastic one contains Mag exsolution lamellae (Figure 13A) that are lacking in the neoblastic one. The porphyroclastic Opx has slightly higher Ca contents (0.023–0.026 a.p.f.u.) than the neoblasts (0.018–0.022 a.p.f.u.) and similar Mg# (0.46–0.52; Figure 9c). The Al contents range from 0.051 to 0.077 in a less coherent trend, but the highest values are preserved in the porphyroclastic cores (up to 0.077 a.p.f.u.; Figure 9d).

The very rare Amp has a grey–greenish color and forms around opaque minerals. The Amp composition, different from that of the mafic lithologies, is tschemarkitic and characterized by Mg# = 0.50–0.57, and (in a.p.f.u.) Ca = 1.82–1.89, Mn = 0.01–0.02, Al = 2.16–2.49, K = 0.31–0.39, Na = 0.31–0.42, Ti = 0.12–0.23, and Cl = 0.01–0.02; F $\leq$ 0.09 (Figure 11). Most opaque minerals in the enderbites are Ilm, in contrast with the mafic granulites.

4.2.3. Mineral Trace Element Composition in Mafic Lithologies

LA-ICP-MS trace element data were collected on clinopyroxene, amphibole, orthopyroxene, and plagioclase from the most promising mafic lithologies, i.e., a foliated variety of the mafic granulite in the Ivrea town area (sample IZ21-20a), a typical, homogenous mafic granulite lacking foliation with a uniform mineral distribution (sample IZ21-18a), and an Amp-rich mafic granulite located in the proximity of a 4 cm-thick hornblenditic

layer (sample IZ21-17). The trace element composition of each mineral within a sample and across different samples is strikingly homogenous (Figure 14).

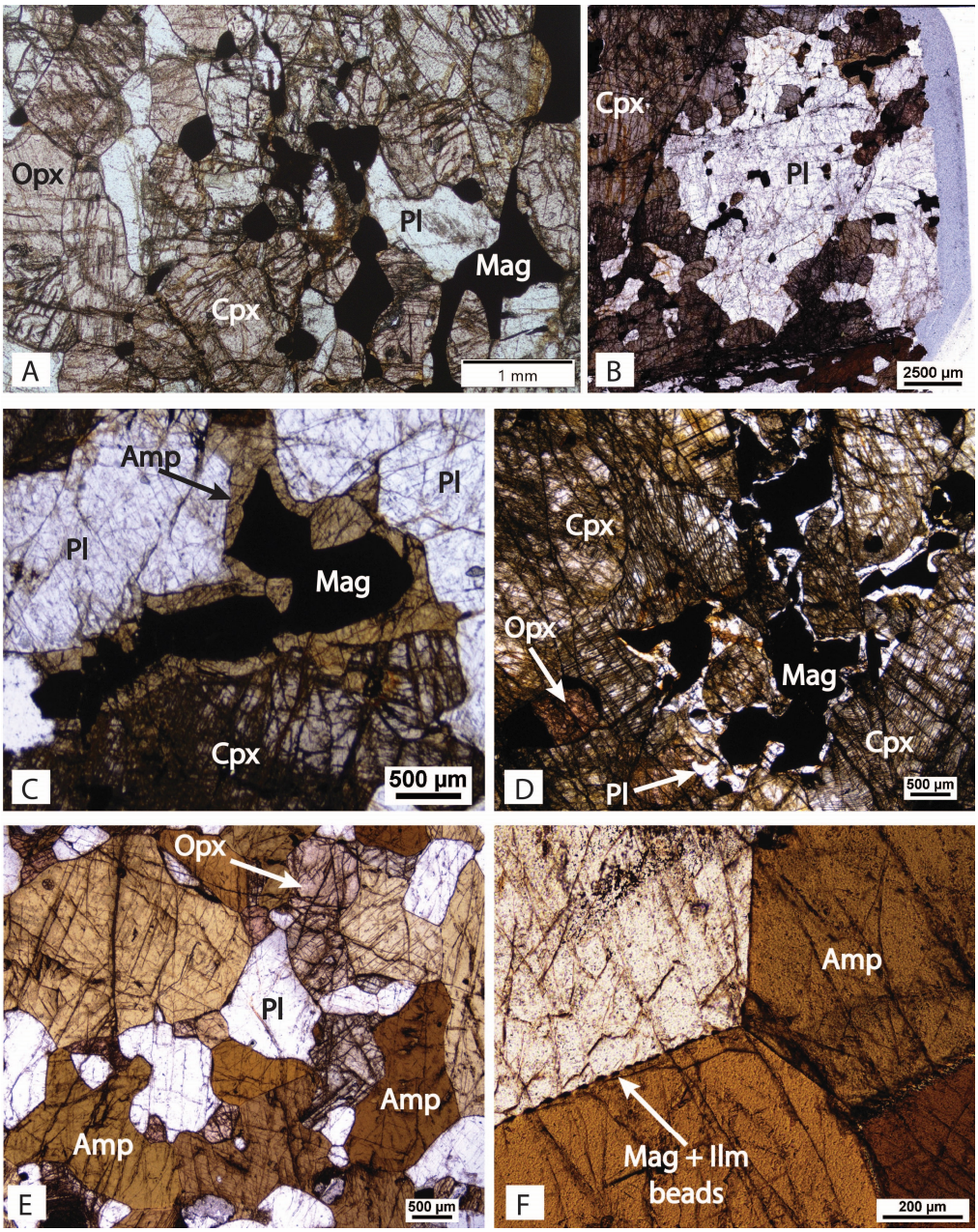

Figure 12. Px-rich layers and Amp-rich dykes and pods under a microscope. (**A**) Typical Px-rich layer consisting of Cpx + Opx + Opq + Pl and showing a granoblastic structure with lobate grain-boundaries, usually evolving toward polygonal ones. Sample IZ23-02b, PPL. (**B**) Coarse-grained Pl and minor Amp cutting and infiltrating a Px-rich layer (for a macroscopic view, see Figure 3D above). Sample IZ21-15a, PPL. (**C**) Interstitial Amp surrounding Mag from a Px-rich layer. Sample IZ21-15a, PPL. (**D**) Interstitial Pl at the contact between Mag and Cpx from a Px-rich layer. Sample IZ21-15a, PPL. (**E**) Pegmatitic Amp from an Amp-rich pod (for a macroscopic view, see Figure 5B above) partly replacing Opx of a mafic granulite. Sample IZ21-17, PPL. (**F**) Pegmatitic polygonal Amp, from an Amp-rich pod, with opaque "beads" at the Amp–Amp grain boundaries. Sample IZ21-17, PPL.

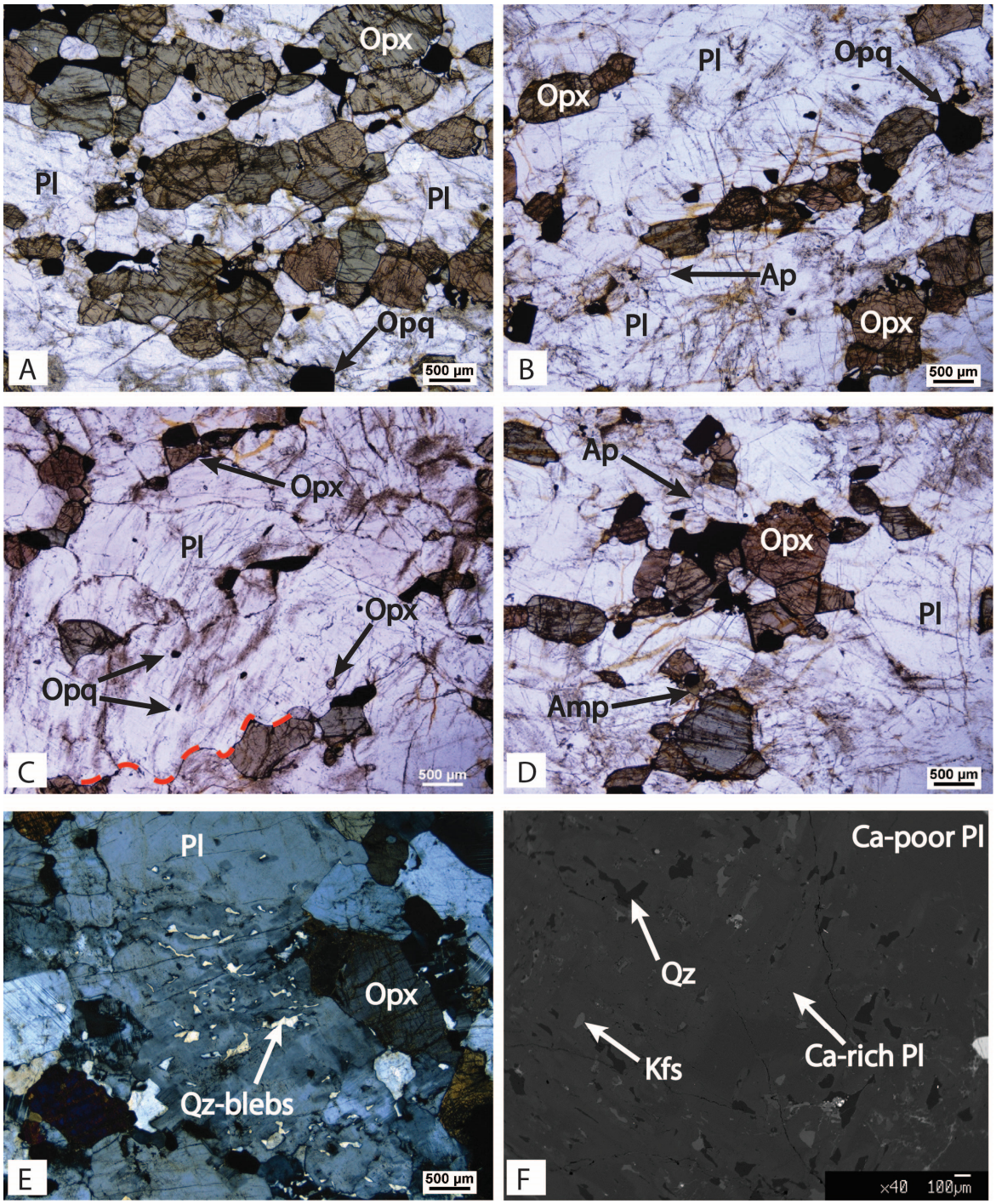

Figure 13. Enderbites under the microscope. (**A**,**B**) Enderbite showing a faint foliation defined by a dimensionally oriented porphyroclastic, exsolution-rich Opx (**A**), or by an elongated aggregate of neoblastic, exsolution-free Opx (**B**). Sample IZ21-04a, PPL. (**C**) Porphyroclastic Pl showing lobate grain-boundaries (red-dashed line) with exsolution-rich Opx. Sample IZ21-01, PPL. (**D**) Neoblastic Opx and Pl showing polygonal granoblastic microstructure. Note the rare green–brown Amp around Opq. Sample IZ21-04a, PPL. (**E**) Pl showing Qz blebs in their interior and at their grain boundaries. Note a change in Pl composition around the blebs. Sample IZ21-02, crossed polarized light (XPL). (**F**) Qz blebs associated with replacement antiperthitic Kfs and with an increase in anorthite component of the hosting Pl. Sample IZ21-01, BSE.

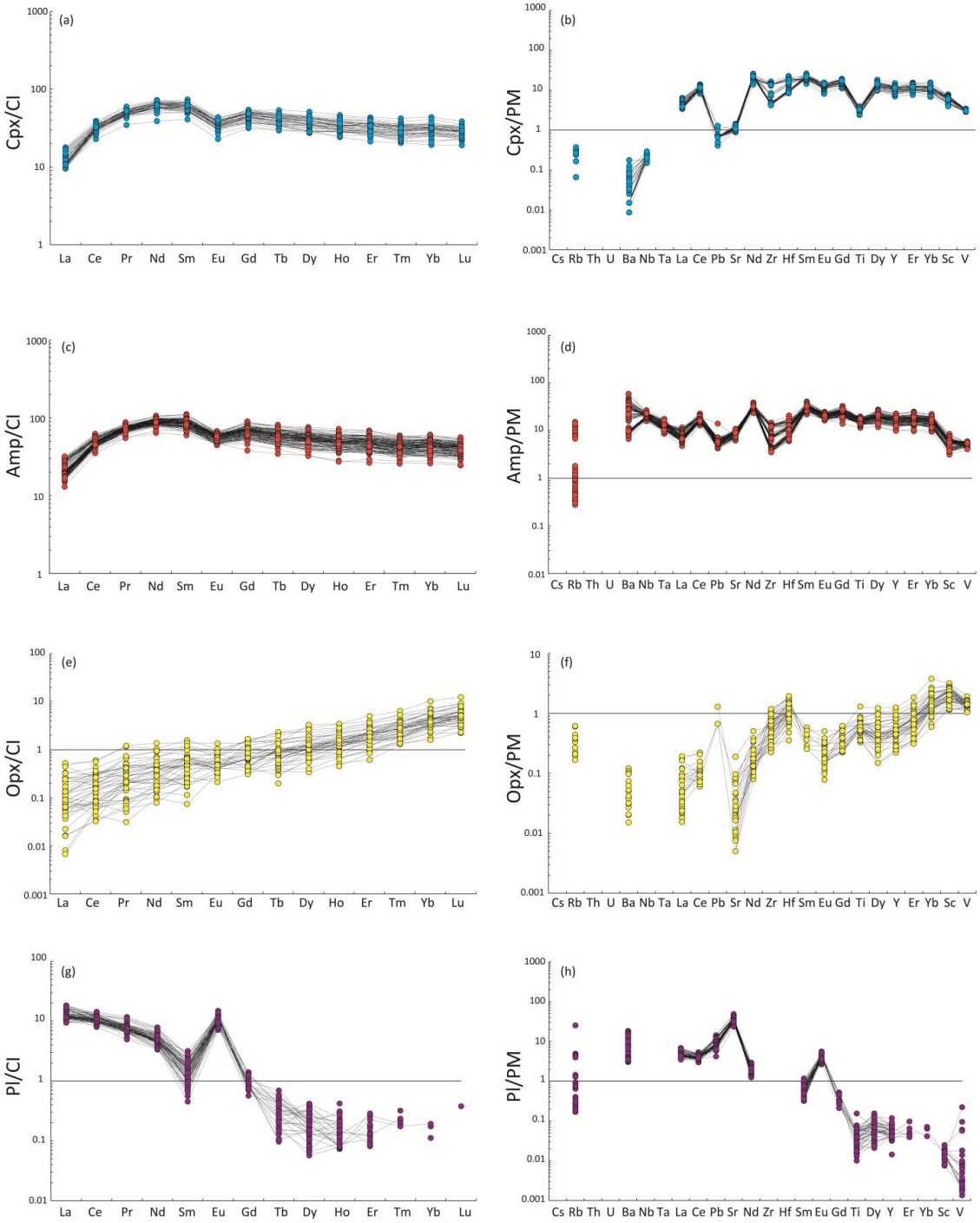

Figure 14. Rare Earth Element (REE) and incompatible trace element patterns of the most abundant minerals in the studied mafic granulites of Ivrea town area: (**a**,**b**) clinopyroxene; (**c**,**d**) amphibole; (**e**,**f**) orthopyroxene and (**g**,**h**) plagioclase. The plots show individual analyses for each mineral. Primitive mantle and CI–chondrite values are from McDonough and Sun [80].

The clinopyroxenes have a chondrite-normalized REE pattern slightly enriched and characterized by a convex–upward LREE distribution, a small negative Eu anomaly, and an almost flat M-to-HREE distribution (Figure 14a). With respect to the primitive mantle, they are poor in HFSE and variably depleted in Rb, Ba, Pb, and Sr, with marked negative anomalies in Pb, Sr, and Ti (Figure 14b). The amphiboles have trace-element compositions pointing to chemical equilibrium with the clinopyroxenes. The amphiboles display REE patterns parallel with the clinopyroxenes, although slightly enriched (Figure 14c), and

LILE and HFSE enrichments with slightly negative anomalies in Pb, Sr, Zr, and Hf, and without Ti anomaly (Figure 14d). The orthopyroxene trace-element contents testify chemical equilibrium with clinopyroxenes and are characterized by slight depletion in LREE and slight enrichments in HREE (Figure 14e), and by depletion in whole trace elements with negative anomalies in Sr (Figure 14f). Additionally, the plagioclase trace-element contents point to chemical equilibrium with the other minerals, i.e., enrichments in LREE, depletion in HREE and HFSE, and positive Ba, Sr, and Eu anomalies (Figure 14g,h).

4.2.4. Thermobarometry

We used amphibole as a geothermobarometer because it is a sensitive mineral to both T and P changes. The recent Ti-in-Amp thermometer ([81]; standard error of the calculation, 1σ, ±35 °C and 2σ ±70 °C [82]) was applied to the mafic granulites as well as the pegmatitic mafic rocks and enderbites (Table S1) because the chemical disequilibrium among the minerals (see discussion) prevents the use of most classical geothermometers (e.g., Amp–Pl thermometer) and makes the use of phase equilibrium modeling questionable [83]. The calculated data indicate T > 900 °C with a peak at 965 °C for the mafic granulites, T > 900 °C with a peak at 933 °C for the pegmatitic mafic rocks, and T < 840 °C with a peak at 810 °C for the enderbites (Figure 15a). Note that the T variation between the mafic granulites and pegmatitic rocks is within the standard error of the calculation. The Si vs. Ti distribution for mafic granulites and pegmatites corresponds to that of UHT granulites, whereas that for enderbites is within the HT field (Figure 15b). Regarding the pressure, the Al^{IV} vs. Al^{VI} distribution is compatible with medium-P granulites (Figure 15c) for all the studied lithologies.

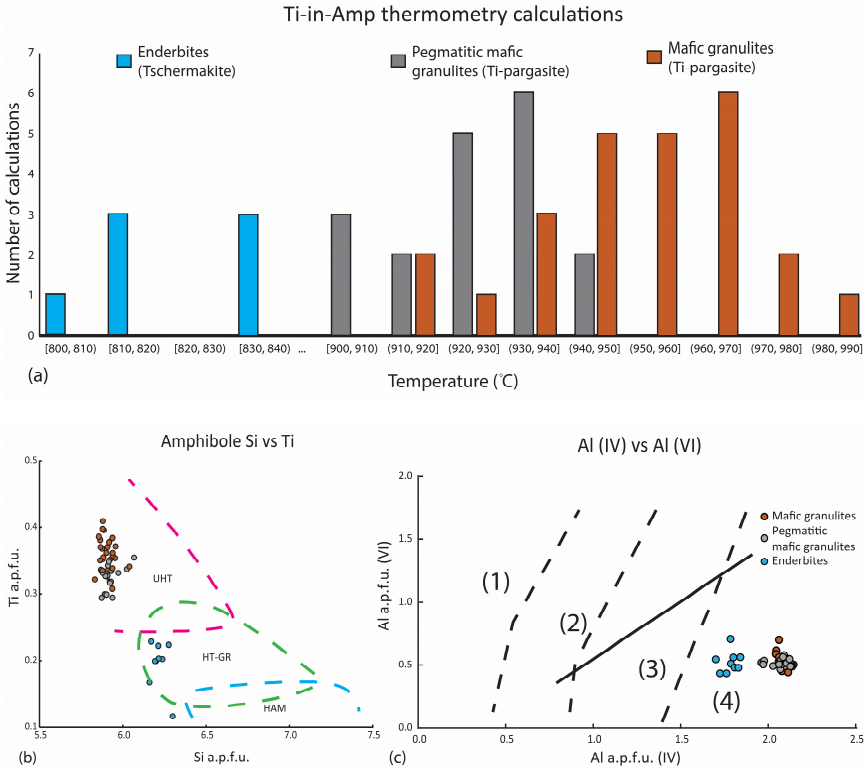

Figure 15. Thermobarometric data from Amp. (**a**) Histograms of the temperatures calculated using the equation of [81]. (**b**) Composition of amphiboles plotted in the Si vs. Ti diagram. The field of high amphibolite (HAM), HT granulite (HT-GR), and UHT granulite facies are from [81]. (**c**) Composition of amphiboles plotted in the Al^{IV} vs. Al^{VI} diagram. The distinction between low-P and high-P amphiboles (solid line) is from [84], and that among amphibole composition from the different metamorphic facies is from [85]: (1) greenschist facies; (2) albite–epidote amphibolite facies; (3) amphibolite facies; (4) granulite facies.

5. Discussion

5.1. Comparison between the Ivrea Granulites and the Other Granulites of the Ivrea–Verbano Zone

Our study indicates that the area of Ivrea town consists of faintly foliated granulites still preserving intrusive field relationships (Figure 1). Most of the area is composed of mafic granulites, with a composition corresponding to Amp–gabbronorite, with local mineral banding parallel to the magmatic foliation and consisting of pyroxenitic layers. Field evidence between mafic granulites and enderbites reveals that the mafic rocks were intruded by enderbitic bodies and, subsequently, by Amp–gabbronoritic to hornblenditic dykes and, finally, by quartz–feldspathic dykes. All the lithologies (excluding quartz–feldspathic dykes) preserve two generations of plagioclase and pyroxenes. The first porphyroclastic generation represents igneous relics, while the second granoblastic generation likely represents the recrystallization that occurred during the 'slow cooling' of the intrusion, due to a prolonged, stationary position at the base of the crust [86].

In the IVZ, mafic granulites occur in the Strona and Sessera Valleys. In the Strona Valley (Figure 1), the metabasites of the Kinzigite formation are interlayered with migmatitic metapelites, quartzites, and marbles (Figure 1), and do not belong to the MC. They have been distinguished, based on their metamorphic grade, which increases towards the Insubric Line, into (a) amphibolites with hornblende, plagioclase, and minor quartz and biotite; (b) garnet-bearing metagabbros with plagioclase, garnet, amphibole, and pyroxene, and (c) 'pyriclastites' (i.e., mafic granulites) with plagioclase, clinopyroxene, orthopyroxene, quartz, and biotite [61]. Middle-to-high-grade metamorphic rocks exhibit migmatitic structures consisting of patchy leucosomes (2–5 cm in size) with quartz–feldspathic composition. In the highest-grade rocks close to the Insubric Line, the degree of partial melting is even higher, making any recognition of field relationships difficult. Partial melting structures in the granulite-facies migmatites of the Kinzigite formation are characterized by interconnected networks of veins or patches of leucosomes consisting of plagioclase, quartz but also peritectic clinopyroxene [33].

The mafic granulites of the Sessera and Sesia Valleys, on the contrary, belong to the MC (Figure 1). Those belonging to the LMC range from Amp–gabbro to gabbronorite in composition and constitute an intermingling structure with leucocratic charnockites, enderbites, ultramafic rocks (pyroxenites and peridotites sequences similar to those of Rocca d'Argimonia; [41,43]), and to Amp-rich pods, and lenses (Figure 1). The lithologies of the LMC are characterized by the granoblastic recrystallization of the former magmatic mineral assemblage given to the slow cooling of the Mafic Complex [63]. On the contrary, the UMC (Figure 1) consists of homogenous diorites, monzodiorites, and gabbros with well-preserved magmatic structures, and occurs in the Sesia Valley [41].

If compared with the rocks from the Strona, Sesia, and Sessera valleys, the granulites of Ivrea town studied in the present work exhibit structures and compositions compatible with those of the LMC, although charnockites and cumulitic peridotites are lacking. The temperatures of around 950 °C are compatible with the temperatures calculated for the lower crust in the Sesia and Strona valleys [63,82]. The LMC is presumed to have been generated by mantle-derived melts with MORB affinity contaminated with melts generated by the partial melting of the hosting metapelites [39]. Enderbitic magma could represent a more evolved mantle-derived magma [39,41,42], possibly by reactive melt flow [3] or by a higher degree of magma mixing or crustal assimilation [39,41,42]. The lack of K-feldspar and biotite in the studied enderbitic samples point to a lack, or a very low degree, of magma mixing or crustal assimilation. The large enderbitic body to the south of Ivrea town could be generated by melt accumulation in low-strain sectors during the activity of high-temperature shear zones, as proposed for the Sesia Valley charnockites [40].

The NE–SW-oriented stronalitic septa show both dimensions (tens or hundreds of meters) and mineral composition (presence of rare K-feldspar and biotite) compatible with the metapelitic bodies belonging to the PBB [33]. In the literature, these septa are interpreted as restitic roof rocks, showing a variable degree of partial melting, incorporated into the MC during the multiple intrusion process coupled with roof rock melting (e.g., [63]). Their

presence in the southeastern part of the studied area could indicate the proximity of the unexposed UMC.

5.2. The Stealth Metasomatism of the Mafic Complex in Ivrea

Microstructures reported in mafic granulites reveal the presence of melt in the late stages of their evolution. The interstitial amphibole with cuspate grain boundaries (Figures 7G and 12C) and the film of interstitial plagioclase around opaques and pyroxenes (Figures 7C–E and 12D) are microstructures indicative of the former presence of melt (i.e., melt pseudomorphs; [87–89]). However, rather than being evidence of in situ partial melting by amphibole breakdown, these melt pseudomorphs are indicative of infiltration of a melt in chemical disequilibrium with the host rock, as testified by the lack of amphibole relics and by the presence of relics of rounded pyroxenes and opaques partly replaced by amphibole with shape preferred orientation (Figures 7G,H and 12C). The infiltration of external melt is also testified by local preservation of a modal increase of amphibole towards the Amp-rich elongated dykes, pods, or lenses, locally pegmatitic, (Figure 5), that reveals a genetic relationship between them and the melt pseudomorphs. The chemical disequilibrium between the infiltrating melt and the host rock is still preserved from the evident difference in the An contents between the interstitial plagioclase (higher An content) and the plagioclase from the older generations (lower An content; Figure 8), and it is partly preserved in the scattered major element composition of clinopyroxenes (Figure 10). Nevertheless, the strongly homogenous trace element content in the clinopyroxene, which perfectly mimics the amphibole one (Figure 14), but also in the orthopyroxene and plagioclase, indicates a strong "cryptic" [90] chemical re-equilibration between the infiltrating melt and some minerals constituting the host rock.

All this evidence point to (i) a metasomatic origin of both the pargasitic amphibole and the An-rich plagioclase induced by chemical disequilibrium between a former "dry" gabbronorite, still rarely preserved (Figure 7A), and a more mafic hydrous–silicate melt (Figure 5); (ii) a syn-tectonic metasomatism occurred at suprasolidus conditions; (iii) a flux of the metasomatic melt along veins/dykes combined with percolation along mineral grain boundaries.

The high volume of Amp–mafic granulites in the studied area (ca. 70 vol% of the mafic granulites) and their high modal amounts of amphibole (up to 45 vol%) indicate that this metasomatic process was pervasive and generated by the melt impregnation of large rock volumes. Because the magmatic amphibole is a common constituent of mafic plutons and its metasomatic origin can be recognized only by microstructural observations and trace element content, the related metasomatism can be named "stealth metasomatism", in agreement with the proposed nomenclature used to characterize the types of mantle metasomatism [90].

The evidence of the metasomatically-driven increase in the modal amount of amphibole in the lower crust up to the generation of hornblendites was already reported by Daczko et al. [1] and Meek et al. [4], and was defined as "reactive infiltration followed by melt flux through an armored zone" by Stuart et al. [2]. Following the process proposed in these studies, the mafic granulites from Ivrea should have experienced a syn-tectonic channeled high-melt flux, enhanced by the former "gabbro glacier"-derived anisotropy [60] that generates hornblendite in the conduits. Starting from the conduits, the melt was transported from the grain scale to the meso-scale by porous flow in an interconnected network promoting melt migration. Because porous flow can occur in the lower crust only in metaigneous rocks and only if the lower crust is particularly hot [91], it is possible that this process could have been active in the MC. Therefore, the porous flow of rising melt promoted the suprasolidus replacement, through grain-scale magmatic assimilation of Cpx of the former dry gabbro-norite into the hydrous Amp–gabbronorite. In this reconstruction, the pegmatitic bodies should represent the final crystallization products of the infiltrating metasomatic melt.

The metasomatic melt was likely hydrous basaltic in composition, as testified by the presence of interstitial amphibole with Mg# 0.70 and plagioclase with labradoritic-bytownitic composition. The increased water content in the melt could be derived from crystal fractionation (e.g., [92–94]) or from a primary feature (e.g., [95] and references therein). It is known that the solubility of water increases at depth and, at 1 GPa, the water concentration in a MORB melt could even reach ca. 15 wt%, depending on temperature (e.g., [96]). Whatever the process, the presence of water in the basaltic metasomatic agent could have been the cause of the channeled flux. The decrease in melt density and viscosity and the increase in melt compressibility (e.g., [96]) could have triggered the rapid rising of the melt from the mantle source into the lower crust by buoyancy along high-permeability channels, likely former shear zones. This channeled melt flow allows the migration of large melt volumes in small rock volumes whose trace-element composition is completely modified but without significant compositional effects outside the channel. The prolonged melt migration in the armored channel [1] allows porous flow percolation likely promoted by the high water content in the infiltrating melt [97] and by the increased connectivity induced by the magmatic assimilation of the minerals, e.g., Cpx, with a consequent decrease in their dihedral angles [90]. This process, allowing percolation of a small melt volume in a large rock volume with pervasive melt–rock interaction, explains the widespread stealth metasomatism in the studied area.

5.3. Geodynamic Implicationsof the Metasomatic Melt

Evidence for multiple infiltration of mafic magmas occurs also in other sectors of the IVZ. In the central IVZ, hornblendite and Amp-rich (45–90 vol%) gabbro and gabbronorite veins or dykes are observed to crosscut peridotite–pyroxenite associations [34]. The amphibole shows Mg# from 0.66 (in Amp–gabbronorite) to 0.82 (in hornblendites), Al_2O_3 = 13.7–15.6 wt%, TiO_2 = 1.3–3.1 wt%, Na_2O = 1.9–2.8 wt%, low HFSE content, and a convex-upward LREE distribution characterized by slight enrichments and lack of negative Eu anomaly. In the northern IVZ, Amp metasomatism of gabbroic rocks by infiltration of external hydrous mafic melts was recently reported by Munnikhuis et al. [19]. The pargasitic amphibole has Mg# = 0.62–0.66, Al_2O_3 = 12.3–13.2 wt%, TiO_2 = 2.06–3.1 wt%, Na_2O = 1.9–2.2 wt%, low HFSE content, and a usually convex–upward LREE distribution characterized by LREE enrichments and small negative Eu anomalies.

A detailed study on the dykes crosscutting the Finero peridotites ([20]; Figure 16) revealed the presence of three kinds of hornblenditic dykes, and associated gabbroic, dioritic, and anorthositic dykes: (i) HFSE-poor hornblendites with pargasitic amphibole characterized by low Mg# (ca. 0.65) and SiO_2 (<ca. 43 wt%), high Al_2O_3 (>ca. 13 wt%) and TiO_2 (<ca. 2.0 wt%), and K_2O at ca. 0.5 wt%; (ii) HFSE-rich hornblendites with pargasitic amphibole characterized by higher Mg# (ca. 0.80) and SiO_2 (up to ca. 46 wt%), lower Al_2O_3 (<ca. 13 wt%) and TiO_2 (ca. 2.5 wt%), and K_2O from ca. 0.4 to ca. 0.7 wt%; (iii) hornblendites with intermediate compositions. The HFSE-poor dykes are considered to have calc–alkaline orogenic affinity and, being derived from partial melting of the metasomatized lithospheric mantle, to belong to the late events (Early Mesozoic) of the post-collisional Variscan magmatism [20]. On the contrary, the subsequent HFSE-rich dykes show an anorogenic affinity, derived from the asthenospheric or deep lithospheric mantle, and should represent the intraplate magmatism in the extensional setting at the beginning of the Alpine cycle. Overall, the major and trace element composition of the pargasitic amphiboles from the Ivrea town area, both those from Amp-rich dykes/pods/lenses and those from hosting mafic granulites, are compatible with the amphiboles reported by Berno et al. [34] and by Munnikhuis et al. [19] and also correspond to those of the HFSE-poor dykes described by Ogunyele et al. ([20]; Figure 17). Possible minor differences in major and trace element contents are likely due to variations in the magma evolution and/or in the mixed crustal component. Thus, the comparison between the data from the Ivrea area and the other sectors of the IVZ indicates that the MC in the southern IVZ experienced a stealth metasomatic event induced by infiltration of post-collisional basaltic magmas.

5.4. Permian Hydration of the Southalpine Lower Crust and Implications for Alpine Magma-Poor Rifting

The field and chemical similarities regarding Amp-rich dykes and hosting Amp-rich mafic granulites in the southern (this study), central (LMC; [34,38,42,43,69]), and northern IVZ (the Finero Complex, e.g., [18–20] and references therein), such as their large volumes deduced by geophysical data [13], point to a widespread Middle Triassic rising of orogenic basaltic magmas. The rising magmas were responsible for the hydration of the whole lowermost part of the IVZ, which is likely composed of more depleted gabbronorite (Figure 41 of [74] and references therein), at least in the southern and central IVZ. The transfer of magmatic heat allowed the infiltrated crust to reach suprasolidus conditions (from supersolidus rocks to melt-poor mush, as described by Sparks et al. [98]), and to exhibit plastic behavior, as also testified by the irregular or gradual contacts of the studied mafic dykes with the hosting rock (Figure 5). On the contrary, the older enderbitic dykes, displaying sharp contacts (Figure 4C,D), indicate that the related colder melt (Figure 14), likely originated by chemical differentiation [3], was injected in a lower crust still characterized by a rigid behavior. Thus, our study suggests a sudden change in the rheological behavior of the lower crust, from rigid to plastic, due to its metasomatic hydration.

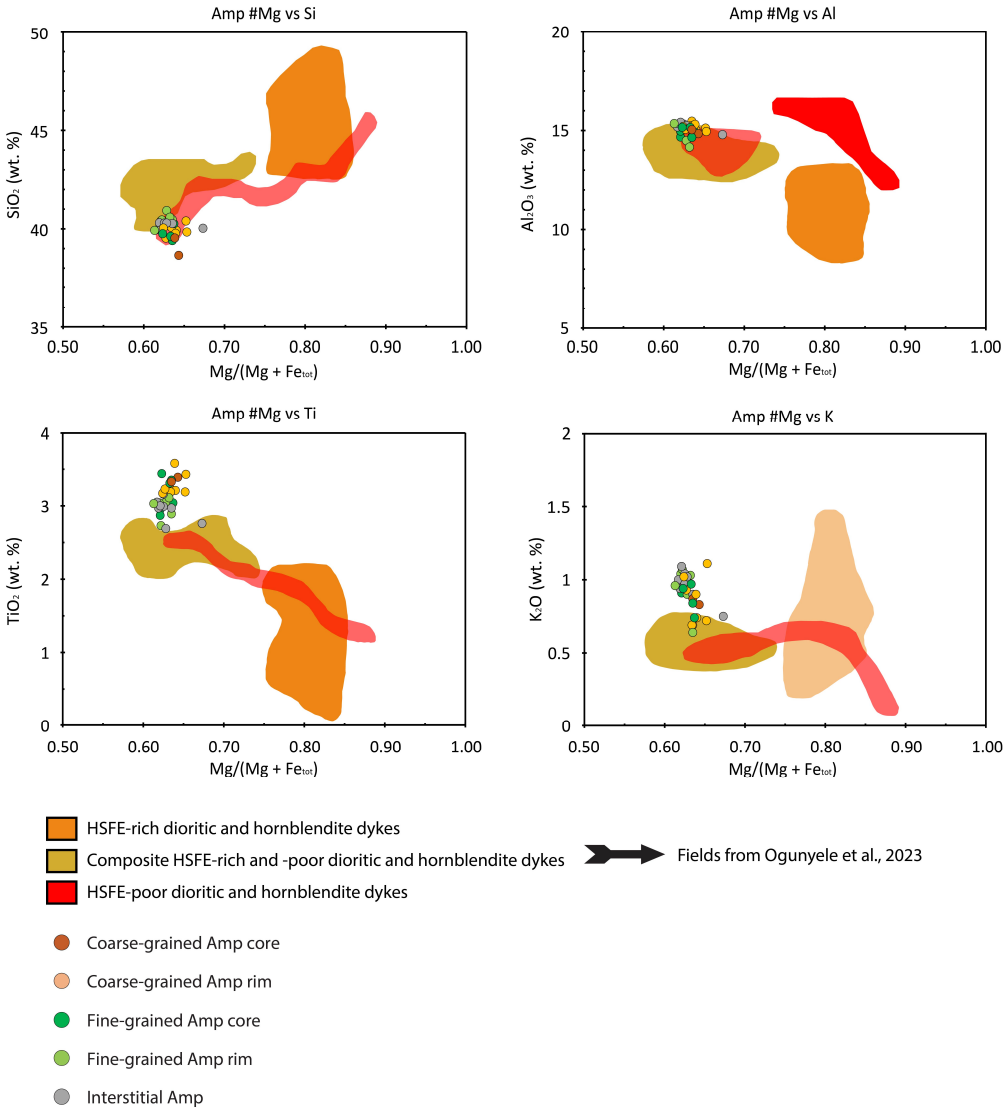

Figure 16. Major element amphibole diagrams comparing this work with the dioritic and hornblenditic dykes of Ogunyele et al. [20] from the Finero Mafic Complex.

Figure 17. Rare Earth Element (REE) and incompatible trace element patterns of the most abundant minerals in the studied mafic granulites of Ivrea town area compared with previous studies from the Finero Mafic Complex [18–20] and Monte Capio area [34], where hornblenditic dykes and associated mafic granulites are reported to have reacted with hydrous basaltic melts. (**a**,**b**) Clinopyroxene; (**c**,**d**) amphibole; (**e**,**f**) orthopyroxene and (**g**,**h**) plagioclase. Primitive mantle and CI–chondrite values are from McDonough and Sun [80].

Considering that the infiltration of the metasomatic hydrous basaltic melts was the last event occurring during the Permian collapse of the Variscan orogen [16,20], the abrupt variation of the lower crust mechanical properties could have had a tectonic role that needs extensive investigation. The metasomatically-induced plasticity of the lower crust could have favored the Triassic thinning of the Variscan crust, the location of the necking domains (e.g., [15] and references therein), and ultimately, the beginning of the Alpine cycle.

At present, the numerical modelization of a magma-poor rifting, like the one responsible for the aperture of the Alpine Tethys (e.g., [15] and references therein), considers a Permian lithospheric section characterized by a strong lower crust made by dry mafic and felsic granulites (e.g., [17,99,100]). Nevertheless, some seismic profiles along rifted margins reveal an indication of ductile deformation of the lower continental crust along shear zones (e.g., [101]).

In the present study, we provide evidence of a continuous infiltration of metasomatic hydrous basalts in the LMC of the IVZ during the end of the Permian. The metasomatic melt infiltrated the former dry mafic plutons at a depth of approximately 25–30 km, migrated in the suprasolidus regime by porous flow, and crystallized [102] at ca. 950 °C. This process generated large volumes of hydrous lower crust at the crust–mantle boundary, and promoted the rising of the isotherms in the middle crust, at least above the largest mafic bodies (Figure 18). A plastic lower crust whose isotherms are perturbed could represent the necessary conditions to activate the intense deformations during the stretching and necking phases of the rifting.

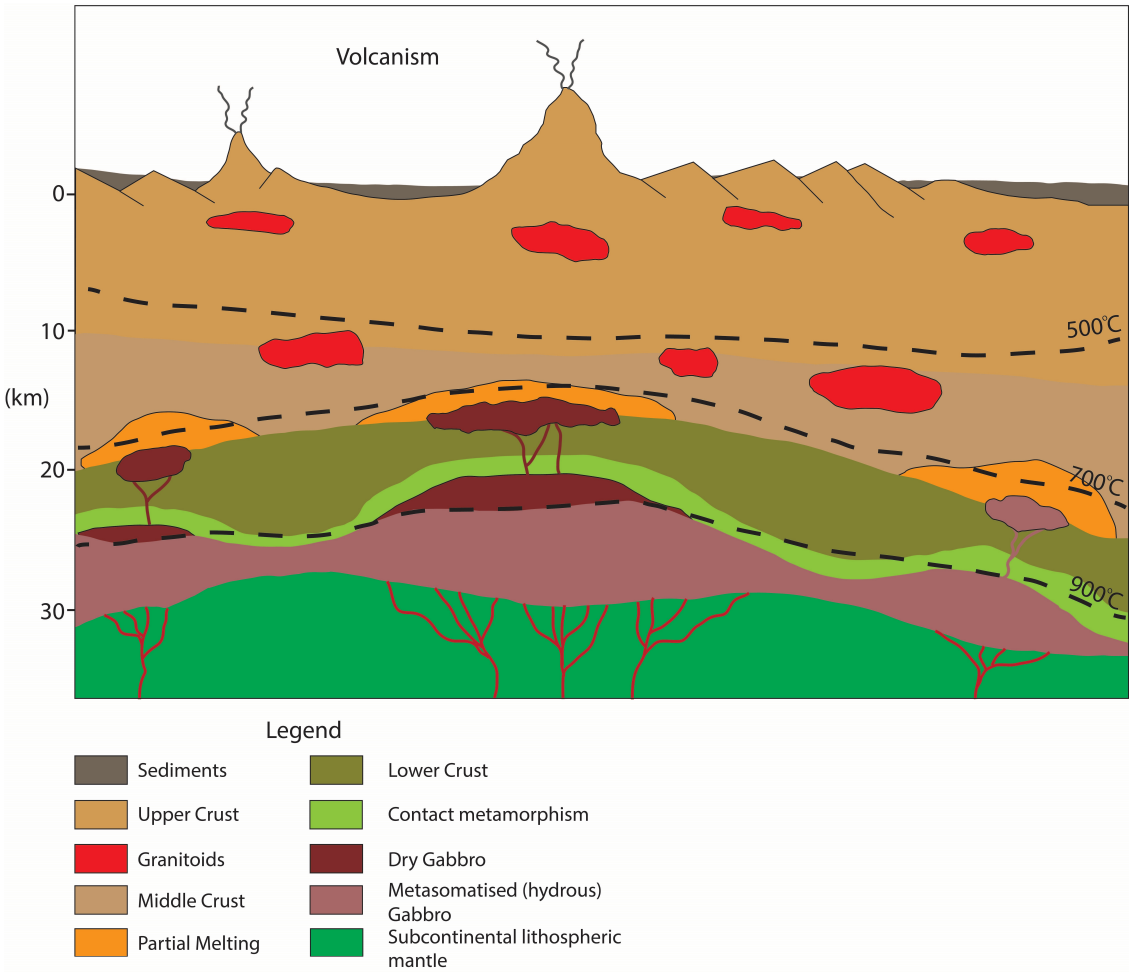

Figure 18. Tectono–thermal sketch of the late-Variscan extension (310–270 Ma) in the Alpine Tethys realm. The isotherm locations are approximate. Modified after Wyatt et al. [36], Manatschal et al. [103], Petri et al. [104], and Real et al. [105].

6. Conclusions

The present work describes the granulites occurring in the southern IVZ (Ivrea town area) and the evidence of melt–rock interactions occurring in the mafic lithologies. The main results are as follows:

- The granulites of the southern IVZ show many similarities with those belonging to the LMC of the central IVZ (Sessera Valley) and are supposed to be genetically similar to them, although with a possible lower degree of crustal contamination. The presence of stronalitic septa could indicate the proximity of a not-outcropping UMC to the southeast.
- The interstitial pargasitic amphibole and An-rich plagioclase in the mafic granulites have a metasomatic origin (stealth metasomatism) and were derived by the supra-solidus interactions between the former dry gabbro–norite with a more mafic hydrous–silicate melt that infiltrated along channels (now hornblenditic dykes) and then percolated along grain boundaries.
- The metasomatic melt likely corresponds to the Early-Mesozoic post-collisional orogenic basaltic magmas, whose infiltration is well documented in the northern IVZ (Finero area).
- The metasomatic event is responsible for the hydration of large volumes of the thick hot lower crust and for the changes in rheology of this crustal level.

Supplementary Materials: The following supporting information can be downloaded at: https://www.mdpi.com/article/10.3390/geosciences14080218/s1, Table S1: Supplementary table of representative mineral chemistry analyses of the major oxides; Table S2: Supplementary table of representative spot analyses of the trace element concentrations; Table S3: Data reporting table (metadata) for LA-ICP-MS; Table S4: Data quality of BCR-2G and comparison with published values; Table S5: Limits of detection per element for spot LA-ICFP-MS analysis. Figure S1: Classification diagrams of (a) pyroxenes, (b) plagioclase and (c) amphibole.

Author Contributions: Conceptualization, S.K., S.F. and M.L.F.; validation, S.K., S.F. and B.E.K.; formal analysis, S.K., S.F. and B.E.K.; investigation, S.K.; resources, S.K. and S.F.; data curation, S.K.; writing—original draft preparation, S.K. and S.F.; writing—review and editing, S.K., S.F., B.E.K. and M.L.F.; visualization, S.K. and S.F.; supervision, S.F. and M.L.F.; project administration, M.L.F.; funding acquisition, M.L.F. All authors have read and agreed to the published version of the manuscript.

Funding: FluidNET: an MSCA ITN project under the European Union Horizon program (grant agreement No 956127), funded this research.

Data Availability Statement: The original contributions presented in the study are included in the article/Supplementary Materials, further inquiries can be directed to the corresponding authors.

Acknowledgments: The authors thank Andrea Rispledente for helping collect the probe analyses at the University of Milan and two reviewers who helped who improved the clarity of the manuscript.

Conflicts of Interest: The authors declare no conflicts of interest.

References

1. Daczko, N.R.; Piazolo, S.; Meek, U.; Stuart, C.A.; Elliott, V. Hornblendite delineates zones of mass transfer through the lower crust. *Sci. Rep.* **2016**, *6*, 31369. [CrossRef] [PubMed]
2. Stuart, C.A.; Meek, U.; Daczko, N.R.; Piazolo, S.; Huang, J.X. Chemical Signatures of Melt–Rock Interaction in the Root of a Magmatic Arc. *J. Petrol.* **2018**, *59*, 321–340. [CrossRef]
3. Jackson, M.D.; Blundy, J.; Sparks, R.S.J. Chemical differentiation, cold storage and remobilization of magma in the Earth's crust. *Nature* **2018**, *564*, 405–409. [CrossRef] [PubMed]
4. Meek, U.; Piazolo, S.; Daczko, N.R. The field and microstructural signatures of deformation-assisted melt transfer: Insights from magmatic arc lower crust, New Zealand. *J. Metamorph. Geol.* **2019**, *37*, 795–821. [CrossRef]
5. Petterson, M.G. The plutonic crust of Kohistan and volcanic crust of Kohistan–Ladakh, north Pakistan/India: Lessons learned for deep and shallow arc processes. *Geol. Soc. Lond. Spec. Publ.* **2019**, *483*, 123–164. [CrossRef]
6. Jagoutz, O.; Schmidt, M.W. The formation and bulk composition of modern juvenile continental crust: The Kohistan arc. *Chem. Geol.* **2012**, *298*, 79–96. [CrossRef]

7. Behn, M.D.; Kelemen, P.B. Stability of arc lower crust: Insights from the Talkeetna arc section, south central Alaska, and the seismic structure of modern arcs. *J. Geophys. Res. Solid Earth* **2006**, *111*, 38–57. [CrossRef]
8. Greene, A.R.; DeBari, S.M.; Kelemen, P.B.; Blusztajn, J.; Clift, P.D. A Detailed Geochemical Study of Island Arc Crust: The Talkeetna Arc Section, South–Central Alaska. *J. Petrol.* **2006**, *47*, 1051–1093. [CrossRef]
9. Guo, L.; Jagoutz, O.; Shinevar, W.J.; Zhang, H. Formation and composition of the Late Cretaceous Gangdese arc lower crust in southern Tibet. *Contrib. Mineral. Petrol.* **2020**, *175*, 58. [CrossRef]
10. Zhang, Z.; Ding, H.; Palin, R.M.; Dong, X.; Tian, Z.; Chen, Y. The lower crust of the Gangdese magmatic arc, southern Tibet, implication for the growth of continental crust. *Gondwana Res.* **2020**, *77*, 136–146. [CrossRef]
11. Handy, M.R.; Franz, L.; Heller, F.; Janott, B.; Zurbriggen, R. Multistage accretion and exhumation of the continental crust (Ivrea crustal section, Italy and Switzerland). *Tectonics* **1999**, *18*, 1154–1177. [CrossRef]
12. Sinigoi, S.; Quick, J.E.; Demarchi, G.; Peressini, G. The Sesia Magmatic System. *J. Virtual Explor.* **2010**, *36*, 1–33. [CrossRef]
13. Pistone, M.; Ziberna, L.; Hetényi, G.; Scarponi, M.; Zanetti, A.; Müntener, O. Joint Geophysical-Petrological Modeling on the Ivrea Geophysical Body Beneath Valsesia, Italy: Constraints on the Continental Lower Crust. *Geochem. Geophys. Geosyst.* **2020**, *21*, 93–97. [CrossRef]
14. Beltrando, M.; Stockli, D.F.; Decarlis, A.; Manatschal, G. A crustal-scale view at rift localization along the fossil Adriatic margin of the Alpine Tethys preserved in NW Italy. *Tectonics* **2015**, *34*, 1927–1951. [CrossRef]
15. Decarlis, A.; Beltrando, M.; Manatschal, G.; Ferrando, S.; Carosi, R. Architecture of the Distal Piedmont-Ligurian Rifted Margin in NW Italy: Hints for a Flip of the Rift System Polarity. *Tectonics* **2017**, *36*, 2388–2406. [CrossRef]
16. Decarlis, A.; Zanetti, A.; Ogunyele, A.C.; Ceriani, A.; Tribuzio, R. The Ivrea-Verbano tectonic evolution: The role of the crust-mantle interactions in rifting localization. *Earth-Sci. Rev.* **2023**, *238*, 104318. [CrossRef]
17. Petri, B.; Duretz, T.; Mohn, G.; Schmalholz, S.M.; Karner, G.D.; Müntener, O. Thinning mechanisms of heterogeneous continental lithosphere. *Earth Planet. Sci. Lett.* **2019**, *512*, 147–162. [CrossRef]
18. Zanetti, A.; Mazzucchelli, M.; Sinigoi, S.; Giovanardi, T.; Peressini, G.; Fanning, M. SHRIMP U-Pb Zircon Triassic Intrusion Age of the Finero Mafic Complex (Ivrea-Verbano Zone, Western Alps) and its Geodynamic Implications. *J. Petrol.* **2013**, *54*, 2235–2265. [CrossRef]
19. Munnikhuis, J.K.; Daczko, N.R.; Langone, A. Open system reaction between hydrous melt and gabbroic rock in the Finero Mafic Complex. *Lithos* **2023**, *440–441*, 107027. [CrossRef]
20. Ogunyele, A.C.; Bonazzi, M.; Giovanardi, T.; Mazzucchelli, M.; Salters, V.J.M.; Decarlis, A.; Sanfilippo, A.; Zanetti, A. Transition from orogenic-like to anorogenic magmatism in the Southern Alps during the Early Mesozoic: Evidence from elemental and Nd-Sr-Hf-Pb isotope geochemistry of alkali-rich dykes from the Finero Phlogopite Peridotite, Ivrea–Verbano Zone. *Gondwana Res.* **2023**, *129*, 201–219. [CrossRef]
21. Cawthorn, R.G. The amphibole peridotite-metagabbro complex, Finero, northern Italy. *J. Geol.* **1975**, *83*, 437–454. [CrossRef]
22. Coltorti, M.; Siena, F. Mantle tectonite and fractionate peridotite at Finero (Italian Western Alps). *Neues Jahrb. Für Mineral. Abh.* **1984**, *149*, 225–244. Available online: http://pascal-francis.inist.fr/vibad/index.php?action=getRecordDetail&idt=9652079 (accessed on 15 June 2024).
23. Hartmann, G.; Hans Wedepohl, K. The composition of peridotite tectonites from the Ivrea Complex, northern Italy: Residues from melt extraction. *Geochim. Cosmochim. Acta* **1993**, *57*, 1761–1782. [CrossRef]
24. Lu, M.; Hofmann, A.W.; Mazzucchelli, M.; Rivalenti, G. The mafic-ultramafic complex near Finero (Ivrea-Verbano Zone), I. Chemistry of MORB-like magmas. *Chem. Geol.* **1997**, *140*, 207–222. [CrossRef]
25. Lu, M.; Hofmann, A.W.; Mazzucchelli, M.; Rivalenti, G. The mafic-ultramafic complex near Finero (Ivrea-Verbano Zone), II. Geochronology and isotope geochemistry. *Chem. Geol.* **1997**, *140*, 223–235. [CrossRef]
26. Morishita, T.; Hattori, K.H.; Terada, K.; Matsumoto, T.; Yamamoto, K.; Takebe, M.; Ishida, Y.; Tamura, A.; Arai, S. Geochemistry of apatite-rich layers in the Finero phlogopite–peridotite massif (Italian Western Alps) and ion microprobe dating of apatite. *Chem. Geol.* **2008**, *251*, 99–111. [CrossRef]
27. Siena, F.; Coltorti, M. The petrogenesis of a hydrated mafic-ultramafic complex and the role of amphibole fractionation at Finero (Italian Western Alps). *Neues Jahrb. Für Mineral. Monatshefte* **1989**, *6*, 255–274. Available online: http://pascal-francis.inist.fr/vibad/index.php?action=getRecordDetail&idt=6808512 (accessed on 15 June 2024).
28. Bertolani, M. La petrografia della Valle Strona (Alpi Occidentali Italiane). *Schweiz. Mineral. Und Petrogr. Mitteilungen* **1968**, *48*, 695. Available online: http://pascal-francis.inist.fr/vibad/index.php?action=getRecordDetail&idt=GEODEBRGM6907005097 (accessed on 2 June 2024).
29. Carvalho, B.B.; Bartoli, O.; Ferri, F.; Cesare, B.; Ferrero, S.; Remusat, L.; Capizzi, L.S.; Poli, S. Anatexis and fluid regime of the deep continental crust: New clues from melt and fluid inclusions in metapelitic migmatites from Ivrea Zone (NW Italy). *J. Metamorph. Geol.* **2019**, *37*, 951–975. [CrossRef]
30. Franz, L.; Harlov, D.E. High-Grade K-Feldspar Veining in Granulites from the Ivrea-Verbano Zone, Northern Italy: Fluid Flow in the Lower Crust and Implications for Granulite Facies Genesis. *J. Geol.* **1998**, *106*, 455–472. [CrossRef]
31. Harlov, D.E. Review of petrographic and mineralogical evidence for fluid induced dehydration of the mafic lower crust: Could there be a relationship between granitoids and granulite facies xenoliths in the Variscan belt? *Z. Geol. Wiss.* **2002**, *30*, 13–36.
32. Henk, A.; Franz, L.; Teufel, S.; Oncken, O. Magmatic Underplating, Extension, and Crustal Reequilibration: Insights from a Cross-Section through the Ivrea Zone and Strona-Ceneri Zone, Northern Italy. *J. Geol.* **1997**, *105*, 367–378. [CrossRef]

33. Kunz, B.E.; Johnson, T.E.; White, R.W.; Redler, C. Partial melting of metabasic rocks in Val Strona di Omegna, Ivrea Zone, northern Italy. *Lithos* **2014**, *190–191*, 1–12. [CrossRef]
34. Berno, D.; Tribuzio, R.; Zanetti, A.; Hérmond, C. Evolution of mantle melts intruding the lowermost continental crust: Constraints from the Monte Capio–Alpe Cevia mafc–ultramafc sequences (Ivrea–Verbano Zone, northern Italy). *Contrib. Miner. Pet.* **2020**, *175*, 2. [CrossRef]
35. Williams, M.A.; Kelsey, D.E.; Rubatto, D. Thorium zoning in monazite: A case study from the Ivrea–Verbano zone, NW Italy. *J. Metamorph. Geol.* **2022**, *40*, 1015–1042. [CrossRef]
36. Wyatt, D.C.; Smye, A.J.; Garber, J.M.; Hacker, B.R. Assembly and Tectonic Evolution of Continental Lower Crust: Monazite Petrochronology of the Ivrea-Verbano Zone (Val Strona di Omegna). *Tectonics* **2022**, *41*, e2021TC006841. [CrossRef]
37. Barboza, S.A.; Bergantz, G.W.; Brown, M. Regional granulite facies metamorphism in the Ivrea zone: Is the Mafic Complex the smoking gun or a red herring? *Geology* **1999**, *27*, 447–450. [CrossRef]
38. Sinigoi, S.; Quick, J.E.; Clemens-Knott, D.; Mayer, A.; Demarchi, G.; Mazzucchelli, M.; Negrini, L.; Rivalenti, G. Chemical evolution of a large mafic intrusion in the lower crust, Ivrea-Verbano Zone, northern Italy. *J. Geophys. Res.* **1994**, *99*, 21575–21590. [CrossRef]
39. Sinigoi, S.; Quick, J.E.; Demarchi, G.; Klötzli, U. The role of crustal fertility in the generation of large silicic magmatic systems triggered by intrusion of mantle magma in the deep crust. *Contrib. Miner. Pet.* **2011**, *162*, 691–707. [CrossRef]
40. Snoke, A.W.; Kalakay, T.J.; Quick, J.E.; Sinigoi, S. Development of a deep-crustal shear zone in response to synteconic intrusion of mafic magma into the lower crust, Ivrea-Verbano zone, Italy. *Earth Planet. Sci. Lett.* **1999**, *166*, 31–45. [CrossRef]
41. Sinigoi, S.; Antonini, P.; Demarchi, G.; Longinelli, A.; Mazzucchelli, M.; Negrini, L.; Rivalenti, G. Intractions of mantle and crustal magmas in the southern part of the Ivrea Zone (Italy). *Contrib. Miner. Pet.* **1991**, *108*, 385–395. [CrossRef]
42. Sinigoi, S.; Quick, J.E.; Mayer, A.; Budahn, J. Influence of stretching and density contrasts on the chemical evolution of continental magmas: An example from the Ivrea-Verbano Zone. *Contrib. Miner. Pet.* **1996**, *123*, 238–250. [CrossRef]
43. Tribuzio, R.; Renna, M.R.; Antonicelli, M.; Liu, T.; Wu, F.Y.; Langone, A. The peridotite-pyroxenite sequence of Rocca d'Argimonia (Ivrea-Verbano Zone, Italy): Evidence for reactive melt flow and slow cooling in the lowermost continental crust. *Chem. Geol.* **2023**, *619*, 121315. [CrossRef]
44. Mazzucchelli, M.; Zanetti, A.; Rivalenti, G.; Vannucci, R.; Teixeira Correia, C.; Gaeta Tassinari, C.C. Age and geochemistry of mantle peridotites and diorite dykes from the Baldissero body: Insights into the Paleozoic–Mesozoic evolution of the Southern Alps. *Lithos* **2010**, *119*, 485–500. [CrossRef]
45. Beltrando, M.; Rubatto, D.; Manatschal, G. From passive margins to orogens: The link between ocean-continent transition zones and (ultra)high-pressure metamorphism. *Geology* **2010**, *38*, 559–562. [CrossRef]
46. Simonetti, M.; Langone, A.; Bonazzi, M.; Corvò, S.; Maino, M. Tectono-metamorphic evolution of a post-variscan mid-crustal shear zone in relation to the Tethyan rifting (Ivrea-Verbano Zone, Southern Alps). *J. Struct. Geol.* **2023**, *173*, 104896. [CrossRef]
47. Brodie, K.H.; Rutter, E.H.; Evans, P. On the structure of the Ivrea-Verbano Zone (northern Italy) and its implications for present-day lower continental crust geometry. *Terra Nova* **1992**, *4*, 34–40. [CrossRef]
48. Fountain, D.M. The Ivrea—Verbano and Strona-Ceneri Zones, Northern Italy: A cross-section of the continental crust—New evidence from seismic velocities of rock samples. *Tectonophysics* **1976**, *33*, 145–165. [CrossRef]
49. Mehnert, K. The Ivrea Zone, a model of the deep crust. *N. Jb. Mineral. Abh.* **1975**, *125*, 156–199.
50. Ferrando, S.; Bernoulli, D.; Compagnoni, R. The Canavese zone (internal Western Alps): A distal margin of Adria. *Schweiz. Mineral. Und Petrogr. Mitteilungen* **2004**, *84*, 237–259.
51. Brack, P.; Ulmer, P.; Schmid, S.M. A crustal-scale magmatic system from the Earth's mantle to the Permian surface—Field trip to the area of lower Valsesia and Val d'Ossola (Massiccio dei Laghi, Southern Alps, Northern Italy). *Swiss Bull. Angew. Geol.* **2010**, *15*, 3–21.
52. Kunz, B.E.; White, R.W. Phase equilibrium modelling of the amphibolite to granulite facies transition in metabasic rocks (Ivrea Zone, NW Italy). *J. Metamorph. Geol.* **2019**, *37*, 935–950. [CrossRef]
53. Redler, C.; Johnson, T.E.; White, R.W.; Kunz, B.E. Phase equilibrium constraints on a deep crustal metamorphic field gradient: Metapelitic rocks from the Ivrea Zone (NW Italy). *J. Metamorph. Geol.* **2012**, *30*, 235–254. [CrossRef]
54. Rutter, E.H.; Brodie, K.H.; Evans, P.J. Structural geometry, lower crustal magmatic underplating and lithospheric stretching in the Ivrea-Verbano zone, northern Italy. *J. Struct. Geol.* **1993**, *15*, 647–662. [CrossRef]
55. Schmid, R.; Wood, B.J. Phase relationships in granulitic metapelites from the Ivrea-Verbano zone (Northern Italy). *Contrib. Miner. Pet.* **1976**, *54*, 255–279. [CrossRef]
56. Sills, J.D.; Tarney, J. Petrogenesis and tectonic significance of amphibolites interlayered with metasedimentary gneisses in the Ivrea Zone, Southern Alps, Northwest Italy. *Tectonophysics* **1984**, *107*, 187–206. [CrossRef]
57. Zingg, A. Regional metamorphism in the Ivrea zone (Southern Alps, N-Italy): Field and microscopic investigations. *Schweiz. Mineral. Und Petrogr. Mitteilungen* **1980**, *60*, 153–179. [CrossRef]
58. Schnetger, B. Partial melting during the evolution of the amphibolite- to granulite-facies gneisses of the Ivrea Zone, northern Italy. *Chem. Geol.* **1994**, *113*, 71–101. [CrossRef]
59. Redler, C.; White, R.W.; Johnson, T.E. Migmatites in the Ivrea Zone (NW Italy): Constraints on partial melting and melt loss in metasedimentary rocks from Val Strona di Omegna. *Lithos* **2013**, *175–176*, 40–53. [CrossRef]

60. Quick, J.E.; Sinigoi, S.; Mayer, A. Emplacement dynamics of a large mafic intrusion in the lower crust, Ivrea-Verbano Zone, northern Italy. *J. Geophys. Res. Solid Earth* **1994**, *99*, 21559–21573. [CrossRef]
61. Reinsch, D. Die Metabasite des Valle Strona (Ivrea Zone) (2.Teil). *Neues Jahrb. Mineral. Abh.* **1973**, *119*, 266–284. Available online: http://pascal-francis.inist.fr/vibad/index.php?action=getRecordDetail&idt=PASCALGEODEBRGM732221277 (accessed on 4 September 2023).
62. Ewing, T.A.; Hermann, J.; Rubatto, D. The robustness of the Zr-in-rutile and Ti-in-zircon thermometers during high-temperature metamorphism (Ivrea-Verbano Zone, northern Italy). *Contrib. Miner. Pet.* **2013**, *165*, 757–779. [CrossRef]
63. Rivalenti, G.; Garuti, G.; Rossi, A.; Siena, F.; Sinigoi, S. Existence of Different Peridotite Types and of a Layered Igneous Complex in the Ivrea Zone of the Western Alps. *J. Petrol.* **1981**, *22*, 127–153. [CrossRef]
64. Sills, J.D. Granulite facies metamorphism in the Ivrea zone, N.W. Italy. *Schweiz. Mineral. Und Petrogr. Mitteilungen.* **1984**, *64*, 169–191. Available online: http://pascal-francis.inist.fr/vibad/index.php?action=getRecordDetail&idt=8976794 (accessed on 5 September 2023).
65. Peressini, G.; Quick, J.E.; Sinigoi, S.; Hofmann, A.W.; Fanning, M. Duration of a large mafic intrusion and heat transfer in the lower crust: A SHRIMP U–Pb zircon study in the Ivrea–Verbano Zone (Western Alps, Italy). *J. Petrol.* **2007**, *48*, 1185–1218. [CrossRef]
66. Barboza, S.A.; Bergantz, G.W. Metamorphism and Anatexis in the Mafic Complex Contact Aureole, Ivrea Zone, Northern Italy. *J. Petrol.* **2000**, *41*, 1307–1327. [CrossRef]
67. Quick, J.E.; Sinigoi, S.; Negrini, L.; Demarchi, G.; Mayer, A. Synmagmatic deformation in the underplated igneous complex of the Ivrea-Verbano zone. *Geology* **1992**, *20*, 613–616. [CrossRef]
68. Rivalenti, G. The origin of the Ivrea-Verbano basic formation (western Italian Alps)-whole rock geochemistry. *Boll. Soc. Geol. Ital.* **1975**, *94*, 1149–1186.
69. Sinigoi, S.; Quick, J.E.; Mayer, A.; Demarchi, G. Density-controlled assimilation of underplated crust, Ivrea-Verbano zone, Italy. *Earth Planet. Sci. Lett.* **1995**, *129*, 183–191. [CrossRef]
70. Karakas, O.; Wotzlaw, J.F.; Guillong, M.; Ulmer, P.; Brack, P.; Economos, R.; Bergantz, G.W.; Sinigoi, S.; Bachmann, O. The pace of crustal-scale magma accretion and differentiation beneath silicic caldera volcanoes. *Geology* **2019**, *47*, 719–723. [CrossRef]
71. Mazzucchelli, M.; Rivalenti, G.; Brunelli, D.; Zanetti, A.; Boari, E. Formation of highly refractory dunite by focused percolation of pyroxenite-derived melt in the Balmuccia peridotite Massif (Italy). *J. Petrol.* **2009**, *50*, 1205–1233. [CrossRef]
72. Quick, J.E.; Sinigoi, S.; Snoke, A.W.; Kalakay, T.J.; Mayer, A.; Peressini, G. *Geologic Map of the Southern Ivrea-Verbano Zone, Northwestern Italy*; Map No. 2776; USGS: Reston, VA, USA, 2003. [CrossRef]
73. Shervais, J.W. Ultramafic layers in the alpine-type lherzolite massif at Balmuccia, NW Italy. Memorie di Scienze Geologiche. *Univ. Padova* **1979**, *33*, 135.
74. Mazzucchelli, M.; Quick, J.E.; Sinigoi, S.; Zanetti, A.; Giovanardi, T. Igneous evolutions across the Ivrea crustal section: The Permian Sesia Magmatic System and the Triassic Finero intrusion and mantle. *Geol. Field Trips* **2014**, *6*, 1–98. [CrossRef]
75. Ulmer, P. *NORM-Program for Cation and Oxygen Mineral Norms: Computer Library*; Institute fûr Mineralogie und Petrographie, ETH-Zentrum: Zürich, Switzerland, 1986.
76. Paton, C.; Hellstrom, J.; Paul, B.; Woodhead, J.; Hergt, J. Iolite: Freeware for the visualisation and processing of mass spectrometric data. *J. Anal. At. Spectrom.* **2011**, *26*, 2508–2518. [CrossRef]
77. Jenner, F.E.; O'Neill, H.S.C. Major and trace analysis of basaltic glasses by laser-ablation ICP-MS. *Geochem. Geophys. Geosyst.* **2012**, *13*, 1–17. [CrossRef]
78. Whitney, D.L.; Evans, B.W. Abbreviations for names of rock-forming minerals. *Am. Mineral.* **2010**, *95*, 185–187. [CrossRef]
79. Le Maitre, R.W.; Streckeisen, A.; Zanettin, B.; Le Bas, M.J.; Bonin, B.; Bateman, P. *Igneous Rocks: A classification and Glossary of Terms: Recommendations of the International Union of Geological Sciences Subcommission on the Systematics of Igneous Rocks*; Cambridge University Press: Cambridge, UK, 2005.
80. McDonough, W.F.; Sun, S.S. The composition of the Earth. *Chem. Geol.* **1995**, *120*, 223–253. [CrossRef]
81. Liao, Y.; Wei, C.; Rehman, H.U. Titanium in calcium amphibole: Behavior and thermometry. *Am. Mineral.* **2021**, *106*, 180–191. [CrossRef]
82. Bartoli, O.; Carvalho, B.B.; Farina, F. Effectiveness of Ti-in-amphibole thermometry and performance of different thermometers across lower continental crust up to UHT metamorphism. *Contrib. Miner. Pet.* **2024**, *179*, 65. [CrossRef]
83. Goncalves, P.; Marquer, D.; Oliot, E.; Durand, C. Thermodynamic Modeling and Thermobarometry of Metasomatized Rocks. In *Metasomatism and the Chemical Transformation of Rock*, 1st ed.; Harlow, D.E., Austrheim, H., Eds.; Springer: Berlin/Heidelberg, Germany, 2013; pp. 53–91. [CrossRef]
84. Raase, P. Al and Ti contents of hornblende, indicators of pressure and temperature of regional metamorphism. *Contrib. Miner. Pet.* **1974**, *45*, 231–236. [CrossRef]
85. Zakrutkin, V.V. The evolution of amphiboles during metamorphism. *Zap. Vsesoyuznovo Mineral. Obshchestva* **1968**, *96*, 13–23.
86. Vernon, R.H.; Collins, W.J.; Cook, N.D.J. Metamorphism and deformation of mafic and felsic rocks in a magma transfer zone, Stewart Island, New Zealand. *J. Metamorph. Geol.* **2012**, *30*, 473–488. [CrossRef]
87. Vernon, R.H. Microstructures of melt-bearing regional metamorphic rocks. In *Origin and Evolution of Precambrian High-Grade Gneiss Terranes, with Special Emphasis on the Limpopo Complex of Southern Africa*; Van Reenen, D.D., Kramers, J.D., McCourt, S., Perchuk, L.L., Eds.; The Geological Society of America: Colorado, CO, USA, 2011; Volume 207, pp. 1–11.

88. Holness, M.B.; Sawyer, E.W. On the pseudomorphing of melt-filled pores during the crystallization of migmatites. *J. Petrol.* **2008**, *49*, 1343–1363. [CrossRef]
89. Holness, M.B.; Cesare, B.; Sawyer, E.W. Melted rocks under the microscope: Microstructures and their interpretation. *Elements* **2011**, *7*, 247–252. [CrossRef]
90. O'Reilly, S.Y.; Griffin, W.L. Mantle Metasomatism. In *Metasomatism and the Chemical Transformation of Rock*, 1st ed.; Harlow, D.E., Austrheim, H., Eds.; Springer: Berlin/Heidelberg, Germany, 2013; pp. 471–534.
91. Maierová, P.; Hasalová, P.; Schulmann, K.; Štípská, P.; Souček, O. Porous melt flow in continental crust-A numerical modeling study. *J. Geophys. Res. Solid Earth* **2023**, *128*, e2023JB026523. [CrossRef]
92. Rudnick, R.L. Making continental crust. *Nature* **1995**, *378*, 571–578. [CrossRef]
93. Sisson, T.W.; Ratajeski, K.; Hankins, W.B.; Glazner, A.F. Voluminous granitic magmas from common basaltic sources. *Contrib. Miner. Pet.* **2005**, *148*, 635–661. [CrossRef]
94. Keller, B.C.; Schoene, B.; Barbonu, M.; Samperton, K.M.; Husson, J.M. Volcanic–plutonic parity and the differentiation of the continental crust. *Nature* **2015**, *523*, 301–307. [CrossRef]
95. Kovács, I.J.; Liptai, N.; Koptev, A.; Cloetingh, S.A.; Lange, T.P.; Maţenco, L.; Szakács, A.; Radulian, M.; Berkesi, M.; Patkó, L.; et al. The 'pargasosphere' hypothesis: Looking at global plate tectonics from a new perspective. *Global Planet. Chang.* **2021**, *204*, 103547. [CrossRef]
96. Manning, C.E. The influence of pressure on the properties and origins of hydrous silicate liquids in Earth's interior. In *Magmas under Pressure*; Elsevier: Amsterdam, The Netherlands, 2018; pp. 83–113. [CrossRef]
97. Fujii, N.; Osamura, K.; Takahashi, E. Effect of water saturation on the distribution of partial melt in the Olivine-Pyroxene-Plagioclase System. *J. Geophys. Res.* **1986**, *91*, 9253–9259. [CrossRef]
98. Sparks, R.S.J.; Annen, C.; Blundy, J.D.; Cashman, K.V.; Rust, A.C.; Jackson, M.D. Formation and dynamics of magma reservoirs. *Philos. Trans. R. Soc. Ser. A Math. Phys. Eng. Sci.* **2019**, *377*, 20180019. [CrossRef] [PubMed]
99. Müntener, O.; Hermann, J.; Trommsdorff, V. Cooling History and Exhumation of Lower-Crustal Granulite and Upper Mantle (Malenco, Eastern Central Alps). *J. Petrol.* **2000**, *41*, 175–200. [CrossRef]
100. Chenin, P.; Manatschal, G.; Decarlis, A.; Schmalholz, S.M.; Duretz, T.; Beltrando, M. Emersion of Distal Domains in Advanced Stages of Continental Rifting Explained by Asynchronous Crust and Mantle Necking. *Geochem Geophys. Geosyst.* **2019**, *20*, 3821–3840. [CrossRef]
101. Clerc, C.; Ringenbach, J.C.; Jolivet, L.; Ballard, J.F. Rifted margins: Ductile deformation, boudinage, continentward-dipping normal faults and the role of the weak lower crust. *Gondwana Res.* **2018**, *53*, 20–40. [CrossRef]
102. Lykins, R.W.; Jenkins, D.M. Experimental determination of pargasite stability relations in the presence of orthopyroxene. *Contrib. Miner. Pet.* **1992**, *112*, 405–413. [CrossRef]
103. Manatschal, G.; Chenin, P.; Ulrich, M.; Petri, B.; Morin, M.; Ballay, M. Tectono-magmatic evolution during the extensional phase of a Wilson Cycle: A review of the Alpine Tethys case and implications for Atlantic-type margins. *Ital. J. Geosci.* **2023**, *142*, 5–27. [CrossRef]
104. Petri, B.; Wijbrans, J.; Mohn, G.; Manatschal, G.; Beltrando, M. Thermal evolution of Permian post-orogenic extension and Jurassic rifting recorded in the Austroalpine basement (SE Switzerland, N Italy). *Lithos* **2023**, *444–445*, 107124. [CrossRef]
105. Real, C.; Fassmer, K.; Carosi, R.; Froitzheim, N.; Rubatto, D.; Groppo, C.; Münker, C.; Ferrando, S. Carboniferous–Triassic tectonic and thermal evolution of the middle crust section of the Dervio–Olgiasca Zone (Southern Alps). *J. Metamorph. Geol.* **2023**, *41*, 685–718. [CrossRef]